

Solar Sails Dynamics and Attitude Control for Satellites and Spacecrafts



Thesis submitted to the Faculty of Engineering & Technology IIU in
partial fulfillment of requirements for the Degree of MS Electronics
Engineering

Submitted by: Abdur Rehman

Registration No: 49-FET/MS-EE/F07

Supervised by: Dr. Sajjad Asghar

INTERNATIONAL ISLAMIC UNIVERSITY

FACULTY OF ENGINEERING & TECHNOLOGY

DEPARTMENT OF ELETRONIC ENGINEERING



Accession No.

7H-8474

MS

523.2

ABS

1. Solar system

2. Solar system; Juvenile literature

DATA ENTERED

Ang
11/04/13



Declaration of Originality

I hereby declare that the work contained in this thesis and the intellectual content of this thesis are the product of my own work. This thesis has not been previously published in any form nor does it contain any verbatim of the published resources which could be treated as infringement of the international copyright law.

I also declare that I do understand the terms 'copyright' and 'plagiarism,' and that in case of any copyright violation or plagiarism found in this work, I will be held fully responsible of the consequences of any such violation.

Signature: 

Name: Abdur Rehman

Date: 11th November, 2010

Place: IIU Islamabad

Certificate of Approval

This is to certify that the work contained in this thesis entitled

“Solar Sails Dynamics and Attitude Control for Satellites and Spacecrafts”

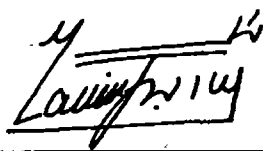
was carried out by

Abdur Rehman

Under my supervision and that in my opinion, it is fully adequate, in scope and quality, for the degree of MS Electronics Engineering from International Islamic University Islamabad (IIUI).


Dean

Dr. Yaseen Chohan
FET, IIUI Islamabad



Chairman/Director

Engg. Suheel Abdullah
FET, IIUI Islamabad



External Examiner

Dr. Aamir Iqbal Bahtti
MAJU, Islamabad



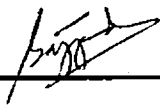
Internal Examiner

Dr. Muhammad Ejaz
Faculty Member IIUI
Islamabad.

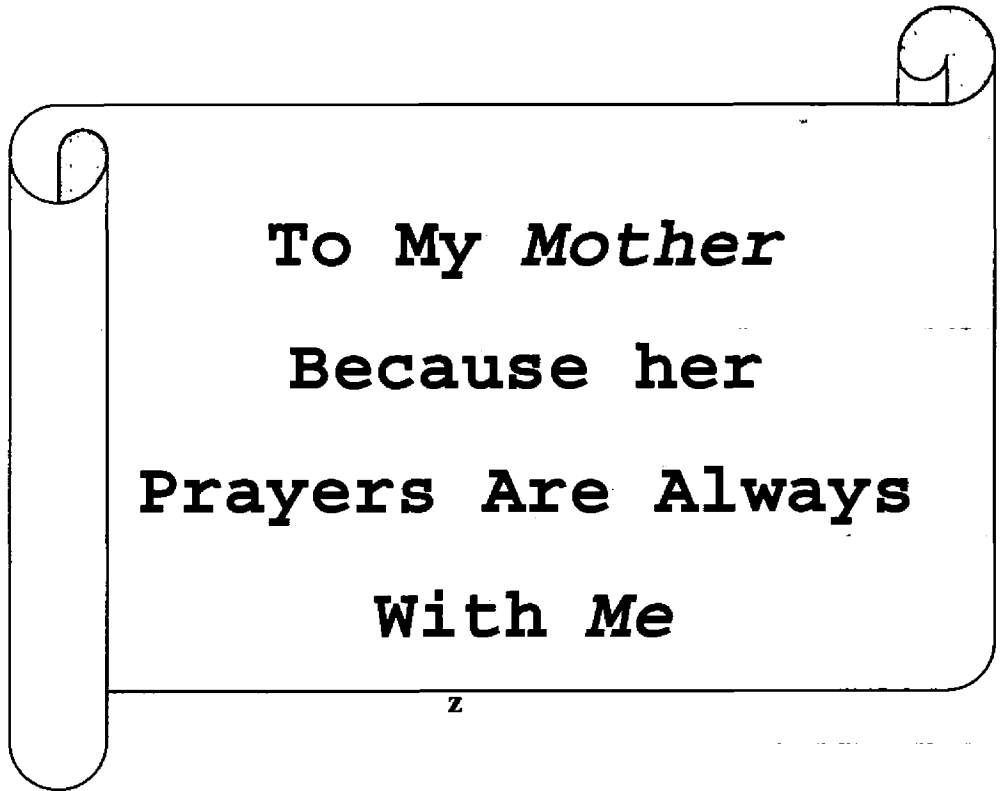


Supervisor

Dr. Sajjad Asghar
NECOM, Islamabad



Dedication



To My Mother
Because her
Prayers Are Always
With Me

Acknowledgments

I wish to acknowledge **Dr. Sajjad Asghar** for his help, encouragement and support during the work on this thesis. I also want to acknowledge **Dr. Yaseen Chohan** (Faculty Dean, IIUI) and **Dr. Muhammad Ejaz** (Faculty member, IIUI) for their assistance and sincere suggestions. I wish to express my acknowledgments to **Dr. Ehsan** (Faculty member, IIUI) for his superb coordination during the project. As always, I remain indebted to my colleagues and friends for their comments and their encouragement.

Abdur Rehman

Table of Contents

ABSTRACT.....	4
CHAPTER 1.....	5
1. INTRODUCTION.....	5
1.1 LITERATURE REVIEW.....	6
1.2 STATEMENT OF NEED.....	8
1.3 PROJECT RUDIMENTS.....	9
1.4 THESIS LAYOUT.....	9
CHAPTER 2.....	10
2. SOLAR RADIATION PRESSURE MODELS.....	10
2.1 SOLAR SAIL CONFIGURATIONS.....	10
2.2 SOLAR RADIATION PRESSURE MODEL.....	12
2.3 SOLAR RADIATION PRESSURE FORCE MODEL.....	14
2.3.1 <i>Perfect reflecting solar sail</i>	14
2.3.2 <i>Non-Perfect reflecting solar sail</i>	18
CHAPTER 3.....	23
3. FUNDAMENTALS OF ATTITUDE DYNAMICS.....	23
3.1 ROTATIONAL KINEMATICS.....	23
3.1.1 <i>Euler Angles</i>	23
3.1.2 <i>Quaternion Representation</i>	26
3.1.3 <i>Modified Rodrigues Parameters</i>	27
3.2 RIGID-BODY DYNAMICS.....	28
3.2.1 <i>Spin Stabilization of Solar Sail Spacecraft</i>	31
3.2.2 <i>Three-axis Stabilized Square Sail Using Control Boom and Control Vans</i>	34
CHAPTER 4.....	42
4. ATTITUDE CONTROLLER DESIGN.....	42
4.1 STATE FEEDBACK CONTROLLER.....	42
4.2 SLIDING MODE CONTROLLER.....	43
4.2.1 <i>Dynamics and kinematics with MRPs</i>	44
4.2.2 <i>Lyapunov's Stability</i>	48
CHAPTER 5.....	50
5. SIMULATION RESULTS.....	50
5.1 SIMULATION RESULTS.....	50
CHAPTER 6.....	61
6. CONCLUSION AND RECOMMENDATIONS FOR FURTHER RESEARCH.....	61
6.1 CONCLUSION.....	61
6.2 RECOMMENDATIONS FOR FUTURE RESEARCH.....	62
REFERENCES.....	63
APPENDIX.....	66

List of Figures

FIGURE 1 – SOLAR SAIL CONFIGURATIONS.....	10
FIGURE 2 – SQUARE SOLAR SAIL WITH CONTROL BOOM.....	11
FIGURE 3 - PERFECT REFLECTING SOLAR SAIL	15
FIGURE 4- PAYLOAD VARIATION WITH SAIL AREA	17
FIGURE 5– NON-PERFECT REFLECTING SOLAR SAIL.....	18
FIGURE 6 - SRP FORCE VARIES WITH PITCH ANGLE OF SAIL	22
FIGURE 7 - EULER ANGLES.....	24
FIGURE 8- REFERENCE FRAME AND MASS ELEMENT.....	29
FIGURE 9 - SIMULATION RESULTS FOR A CM/CP 0.1 M OFFSET.....	33
FIGURE 10- PITCH TORQUE AS A FUNCTION OF ELEVATION AND AZIMUTH	36
FIGURE 11 - YAW TORQUE AS A FUNCTION OF ELEVATION AND AZIMUTH	37
FIGURE 12 - TWO VANS ORIENTATION	38
FIGURE 13- SUN VECTOR IN BODY FRAME.....	38
FIGURE 14 - PITCH TORQUE QS A FUNCTION OF VANE ROATIONS.....	40
FIGURE 15 - ROLL TORQUE AS A FUNCTION OF VANE ROTATIONS.....	41
FIGURE 16: STATE FEEDBACK CONTROLLER	43
FIGURE 17-PD CONTROLLER TORQUES.....	52
FIGURE 18- PD CONTROLLER ANGULAR VELOCITIES.....	53
FIGURE 19- PD CONTROLLER EULER ANGLES	53
FIGURE 20- MODIFIED RODRIGUES PARAMETERS	54
FIGURE 21 – SLIDING MODE TORQUES.....	55
FIGURE 22- SLIDING MODE ANGULAR VELOCITIES	55
FIGURE 23 - SLIDING MODE EULER ANGLES.....	56
FIGURE 24- PHASE PORTRAIT Ω_1 VS P_1	57
FIGURE 25 - PHASE PORTRAIT Ω_2 VS P_2	57
FIGURE 26 - PHASE PORTRAIT Ω_3 VS P_3	58
FIGURE 27 – SLIDING COORDINATE S_1 VS TIME.....	59
FIGURE 28– SLIDING COORDINATE S_2 VS TIME.....	59
FIGURE 29– SLIDING COORDINATE S_3 VS TIME.....	60

List of Tables

<i>TABLE 1- OPTICAL COEFFICIENTS FOR AN AL/CR COATED SAIL</i>	<i>21</i>
<i>TABLE 2- SAIL CHARACTERISTICS.....</i>	<i>33</i>
<i>TABLE 3-SOLAR SAIL CHARACTERISTICS.....</i>	<i>50</i>
<i>TABLE 4- ATTITUDE CONTROL CHARACTERISTICS</i>	<i>51</i>
<i>TABLE 5- SIMULATION PARAMETERS.....</i>	<i>51</i>

Abstract

In this dissertation, we have presented attitude dynamics and control of spacecraft using solar sails. The mathematical model for attitude motion of square solar sail by using solar radiation pressures/forces has been developed. First technique uses control boom for varying moment arm (c_m - c_p offset) whereas the other uses control vanes for deflecting the radiation pressure in order to produce rotational torques. We have used sliding mode approach to design attitude controller using Modified Rodrigues Parameters (MRPs) for sail craft attitude maneuvering. Stability is proved by Lyapunov's theorem with a new Lyapunov candidate function. This approach is successfully tested in MATLAB simulation for both attitude regulation and tracking problem for a square sail example. We have also compared the simulation result for the sliding mode controller with a classical PD control approach using Euler angles. Sliding mode controller is found to be more robust in our simulation results.

Chapter 1

1. Introduction

There is a significant need for advance space propulsion techniques with the potential for dramatic reduction in the cost of access to space, specifically for missions of longer duration e.g., interplanetary missions and travel in the space or for performing long term periodic motions in the space [1]. Sailing, in the most general sense, is the technique of diverting a portion of a momentum flux for the purpose of propelling a vehicle. Sailing boats and ships achieve this with wind sails, which divert a small portion of the massive momentum flux of air. In space, a vehicle called solar sail spacecraft can achieve the same effect by diverting a portion of the massive flux of electromagnetic energy of the Sun and other shining stars using large and light weight mirrored sails. The clear picture of a solar sail is that of a large shining membrane of a thin, highly reflective, film held in tension by some gossamer structure [5] using momentum gained only by reflecting ambient light from the Sun. Solar sail are used to

- Slowly but continuously accelerate satellites and spacecrafts
- Maintain the orbits and increase the life of satellites
- Control the attitude dynamics of satellites and spacecrafts

Since 1950, a lot of research papers have been published on solar sails. These papers have mainly discussed the orbital dynamics of solar sails and the trajectories they could follow around the Sun, the Planets and in the interplanetary space.

During the last three decades, a variety of advanced control systems for spacecrafts have been developed [2]. The recent advancements in this field is like a light weight deployable booms, ultra light sail films and small satellite technologies are spurring a renewed interest in solar sailing [6]. As a result, solar sail missions are being developed and the associated sail craft technologies are growing rapidly. Solar sails have the potential to provide cost effective propellant-less propulsion that enables

longer mission lifetime and access to previously inaccessible orbits. Solar sail mission applications are:

- Inner solar system missions
- Outer solar system missions
- Non-Keplerian orbits
- Autonomous space explorers

In attitude control systems (ACS) of sail craft, solar radiation pressure is used for attitude maneuvering trajectories ([8], [9] & 12). In this thesis, solar sail attitude dynamics and control system will be examined in detail.

In particular, this work presents an overview of sail craft attitude control issues, like simple stabilization concept for countering the significant effect of a solar pressure disturbance torque, caused by an uncertain center-of-mass and center-of-pressure offset, on sail craft stability and pointing vector, low thrust used to control large attitude angles and dynamics due to external disturbances. A sail craft controlled by means of translating and/or tilting sail panels will also be described here. Different attitude control schemes have been compared. The overall study objective is to advance/enhance the existing sail craft attitude control technology so that a sail spaceflight experiment for validating sail attitude stability and controllability and thrust vector pointing and steering performance can be conducted in future.

1.1 Literature Review

For keeping up satellites, space station in their orbits, we need low cost propellant or propellant-less propulsion systems because of the long life of satellites and space systems. The NASA Advanced Propulsion Systems Concepts Program has been discussed in AIAA/ASME/ASEE Joint Propulsion Conference [1]. In Ref. [2] & [4] Bong Wei has discussed the development of attitude control system for solar sail flight mission in a sun-synchronous orbit. The impact on the achievable performance and some key structural characteristics in 100-m square solar sails of various design conditions and parameters is explored. Bong Wei has also discussed different PD and PID control schemes for solar sail craft attitude control like control through cp/cm offset, CMGs, Reaction Wheels or sliding masses etc. Upper-bound performance is

addressed with architecture of manageable mechanics and likely ultimate structural efficiency in this class of sails due to uni-axial tensioning in each quadrant, namely, the stripped sail. Ultra Sail is a next-generation high-risk, high-payoff sail system for the launch, deployment, stabilization and control of very large (km² class) solar sails enabling high payload mass fractions for high ΔV . Ultra Sail is an innovative, non-traditional approach to propulsion technology achieved by combining propulsion and control [3] systems developed for formation-flying micro-satellites with innovative solar sail architecture to achieve controllable sail areas approaching 1 km², sail subsystem area densities approaching 1 g/m², and thrust levels many times those of ion thrusters used for comparable deep space missions. The problem of optimally controlling the sail steering angle of a solar sail spacecraft is an important problem in space trajectories. It is considered by T. S. Jayarman [15] in detail. The optimized orbit transfer time of the solar sail spacecraft is compared with that of an ionic propulsion system in this paper. A comprehensive mathematical formulation of the thrust vector control (TVC) design problem of solar sail spacecraft is described by Bong Wie [16] and mission applications on sun-synchronous orbit are given in ref.[17]. A TVC system is part of an attitude and orbit control system (AOCS) of a sail craft, and it maintains the proper orientation of its solar sail to provide the desired thrust vector pointing. The solar pressure thrust vector direction of a sail craft is often described by its cone and clock angles with respect to a particular orbital reference frame. This paper describes various forms of orbital trajectory equations, which employ two different sets of the cone and clock angles, for the design and simulation of solar sail TVC system. Orbital mechanics concepts and mission application are analyzed by C. R. McInnes in [5]. Likewise the problems of optimality like optimal control law for interplanetary trajectories, optimum orbital control using solar radiation pressure and time-optimal orbit transfer trajectory for solar sail spacecraft has been discussed S.K. Shrivastava, Guido Colasurdo, Berned Dachwald and J.C. Van Der Ha , V.J. Modit in ref. [11],[9],[12] and [10] respectively. A close-loop control design for space craft attitude control with large angle maneuvering and slew rate control using small rotational torques has been developed in recent few years. Bong Wei [4], Valadi S.R [20] , Utkin V.I [21] etc are the big names in this area. They have been used simple feedback control schemes to control the attitude dynamics bounded by various

constraints. Many non-linear dynamic controllers are used to solve the attitude control problem as feedback controller. Crassidis, J.L., Markley, F.L. [18] used non-linear sliding mode controller are an attitude control problem. A variable-structure controller is applied for space craft pointing and regulation. They also design an optimal variable-structure controller with Valadi S.R [20] which uses a feedback linearizing technique and an additional term aimed at dealing with model uncertainty. Robust adaptive variable-structure controllers are the achievements of the recent years as in ref. [22] & [23]. Advance dynamics modeling and analysis of rigid bodies are described in ref. [13], [14] & [24]. M. J. Sidi [24] given a practical engineering approach for the spacecraft dynamics and control. Recently K.D Kamar [25,26] used nonlinear adaptive sliding mode for attitude control of satellite (not a solar sail) using solar radiation pressure. However, they have considered a satellite with two flaps, used to provide the desired control torque only in *pitch direction*. Main propulsion system is solar radiation propulsion. The adaptation law was designed for solar pressure and mass distribution parameters. Defined sliding surface is function of inertial pitch angle and its first and second derivatives.

The main objectives of this dissertation are

- Description of solar sails configurations and dynamics
- Description of physics of solar radiation pressures/forces
- Design of sliding mode control law for three axis attitude control of spacecraft/satellites

Our work is on solar sail spacecraft with main propulsion system and use attitude control to keep the sail on desired trajectories. In this thesis, a control boom and control vans (2 or 4) can be used to generate control torques for *three axes attitude* control. In our approach, we define a sliding plane which is the function of angular velocities and MRPs. Our approach works very well in the presence of external disturbances.

1.2 Statement of Need

Low cost and unlimited propulsion in the space is the dream of man from the ancient times. A renewed interest in the solar sailing due to its potential for propellant-less space propulsion is a major research area in space technology. Solar sails dynamic

modeling and development of attitude control systems for satellites/spacecrafts is the main objective of this thesis.

1.3 Project Rudiments

The pre-requisite to this thesis is the knowledge of solar radiation pressure and force models, rigid body dynamics, solar sail orbital dynamics and fundamentals of control theory.

1.4 Thesis Layout

The formulation of this document comprises of six chapters, including the preliminary *Chapter 1*, giving an overview of the thesis research work.

Solar sail configurations, different designs and solar radiation pressure (SRP) and solar radiation force SRF models are discussed in *Chapter 2*. To understand the control attitude of a satellite and space craft, it is important to comprehend the rotational dynamics. *Chapter 3* gives a brief introduction to rotational kinematics and dynamics of satellites and spacecrafts. Rotational torques produced by actuators for attitude maneuvering and control are also explained in this chapter. *Chapter 4* discussed two control schemes in detail. Robustness and stability analysis has also been carried out for the designed controllers for the attitude control of solar sails using solar radiation pressure and forces. Simulation results of a square solar sail configuration are presented in *Chapter 5*. Comparison of two control scheme over the same problem has been shown with figures. In *Chapter 6*, conclusions of the present work and future work recommendations are described.

Concluding remarks are also given at the end of this chapter followed by some *References* for further study and an *appendix* containing MATLAB codes used for the simulations ends the thesis.

Chapter 2

2. Solar Radiation Pressure Models

2.1 Solar Sail Configurations

The main objective of a solar sail design is to provide a large, flat reflective film which requires a minimum structural support mass [3]. The sail film must be kept flat through the application of tensile forces at the edges of the film. There are three basic types of solar sails ([3] & [5]) which are shown in Figure 1.

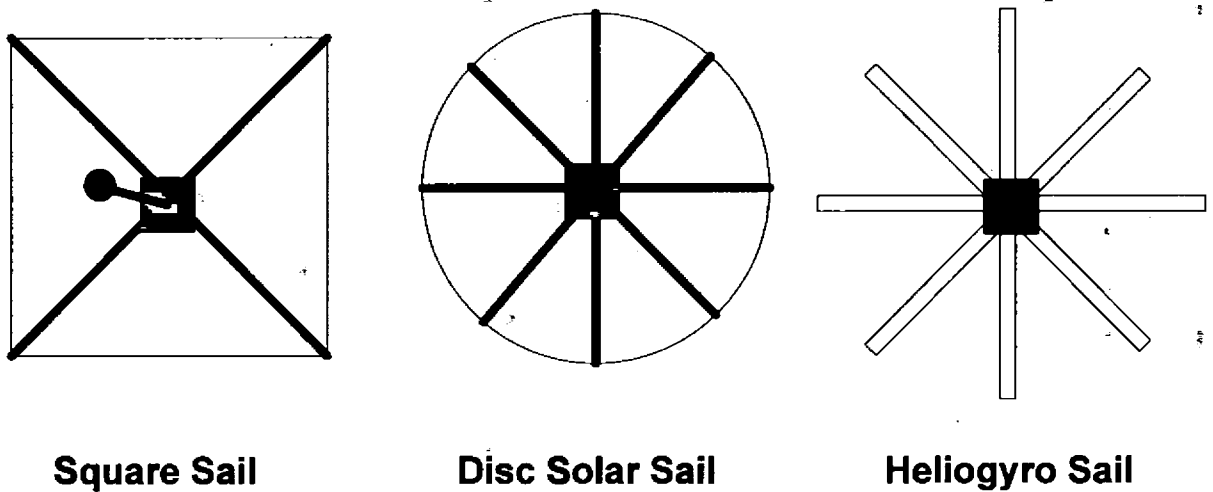


Figure 1 – Solar Sail Configurations

These configurations have their own advantages and disadvantages in terms of control authority, controllability, packing, deployment and maintenance etc. The fundamental objective of any solar sail design is to provide a large sized area (surface area), flatness and high reflective solar film which require a minimum of structural support mass [5]. Keeping the surface of a solar sail flat, we use tensile forces by cantilevered spars or by centripetal forces generated by spinning the solar sail film. These three types of sails are described below:

b) Heliogyro Solar Sail

In this configuration, the solar sail film is divided into a number of long slender blades (8 meter wide, 7.5 km long as in [5]) which are attached to a central load bearing hub shown in Figure 1. The blades are designed in such a way that they produce spin torque and the sail spins slowly which keeps it flat due to spin induced tension. Asymmetric force can produce precision motion in the sail. Such sails are easy to pack and deploy but cannot be used in three axes attitude control.

c) Disc Solar Sail

The intermediate concept between three axes stabilized square sail and heliogyro sail is the disk solar sail. In its design, the triangular film strips are attached with structural bars. The sail is kept flat by using spin induced tension but without such long plates. The attitude control of a rotating disc can be done through torques induced by the offset of the center of mass and center of pressure. The induced torques will precess the spin axes. This precession can be used for orbit raising purpose.

2.2 Solar Radiation Pressure Model

The source of force on solar sails spacecraft is the momentum transported to the spacecraft by radiation energy of the sun ([1] & [5]). In this chapter, the physics of solar radiation pressure will be explained by considering the physical description of momentum transfer process. The quantum description of radiation is as a packet of energy. Photons can be visualized as traveling radially outward from the sun and scattering off the sail, thus imparting their momentum to the sail. According to Planks law, a photon with frequency ν has energy

$$E = h\nu \quad (2.1)$$

In Einstein's view,

$$E^2 = m_0^2 c^4 + p^2 c^2 \quad (2.2)$$

where m_0 is rest mass, p is linear momentum and c is the velocity of light. The intrinsic energy $E_0 = m_0 c^2$ is the energy at rest of a body which is zero in case of a photon. Therefore, the above equation becomes

$$E^2 = p^2 c^2 \Rightarrow E = pc$$

or

$$p = E / c$$

Since the amount of energy transported through area A in time Δt is

$$\Delta E = WA\Delta t$$

Where W is the energy flux (the amount of energy per unit area in unit time).

But

$$\begin{aligned} \Delta p &= \Delta E / c \\ \Delta p &= WA\Delta t / c \\ \frac{1}{A} \cdot \frac{\Delta p}{\Delta t} &= \frac{W}{c} \end{aligned}$$

And we know that rate of change of momentum is force

$$\lim_{\Delta t \rightarrow 0} \frac{\Delta p}{\Delta t} = F$$

But pressure 'Pr' is defined as

$$Pr = \frac{F}{A}$$

Or

$$Pr = \frac{W}{c} \tag{2.3}$$

For perfect reflective solar sail

$$Pr = \frac{2W}{c} \tag{2.4}$$

The energy flux W at a distance ' r ' from the Sun is

$$W = W_E (R_E / r)^2$$

Where $W_E = L_s / 4\pi R_E^2$ is radiation energy flux measured at the earth (1 AU).

$$W = \frac{L_s}{4\pi R_E^2} \cdot \frac{R_E^2}{r^2} = \frac{L_s}{4\pi r^2}$$

where L_s is solar luminosity whose value at 1 AU is 3.856×10^{26} , and R_E is distance from the Sun to the earth (one astronomical unit).

The mean value of $W_E = 1368 \text{ J/s-m}^2$, so putting value of W

$$Pr = \frac{2W_E}{c} \left(\frac{R_E}{r} \right)^2$$

where

$$\frac{W_E}{c} = 4.563 \times 10^{-6} \text{ N/m}^2 \text{ at } 1\text{AU}$$

2.3 Solar Radiation Pressure Force Model

The solar radiation pressure (SRP) forces are generated due to photon impingement on the surface of a solar sail in space. Different assumptions can be made which result in different models for the magnitude and direction of SRP force acting on the sail. Generally, there are three models. The simplest model assumes an ideally reflecting sail surface named as the ideal reflection model (IR). When the solar sail is not ideally reflecting, as in the case of real solar sails, an overall sail efficiency factor ' η ' is typically used in the solar sail related literature [1]. This factor reduces the magnitude of force while leaving the direction unaltered. This is termed as the η -perfect reflection model (η PR). Since real sails are not perfect reflectors due to various reasons, therefore, both the direction and magnitude of the SRP force are different from the ideally reflecting solar sails.

2.3.1 Perfect reflecting solar sail

An analysis of a perfect reflection solar sail (IR) with a square design, as shown in Figure 3, is presented below:

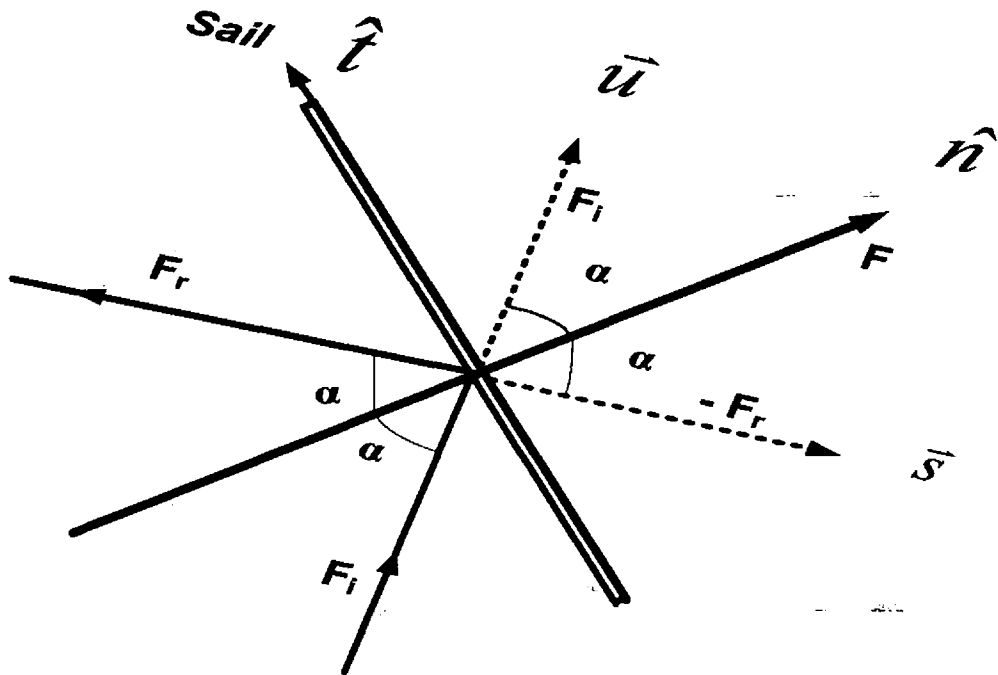


Figure 3 - Perfect Reflecting Solar Sail

For perfect solar sails

$$|\vec{F}_r| \approx |\vec{F}_i|$$

$$\vec{F}_i = \text{Pr } A_s \cos \alpha \vec{u}$$

where A_s is solar sail surface area, α is pitch angle and \vec{u} and \vec{s} are vectors in the directions of incident ray and opposite to reflected ray, respectively. Therefore, the force due to reflecting rays is

$$\vec{F}_r = \text{Pr } A_s \cos \alpha (-\vec{s})$$

So the net force is

$$\vec{F} = -\vec{F}_r + \vec{F}_i$$

$$\vec{F} = \text{Pr } A_s \cos \alpha (\vec{u} + \vec{s})$$

Now

$$\begin{aligned} \vec{u} + \vec{s} &= (\cos \alpha \hat{n} + \sin \alpha \hat{t}) + (\cos \alpha \hat{n} - \sin \alpha \hat{t}) \\ &= 2 \cos \alpha \hat{n} \end{aligned}$$

and

$$\vec{F} = 2Pr A_s \cos^2 \alpha \hat{n} \quad (2.5)$$

is the force on solar sail in normal direction.

Two parameters are used to define the performance of a solar sail. One is characteristic acceleration ' a_c ' and the other is the sail lightness number ' β_0 '.

Characteristic acceleration is defined as

$$a_c = \frac{|\vec{F}|}{m_0} = \frac{2Pr_0 A_s \cos^2 \alpha}{m_0}$$

When $\alpha = 0$, i.e., the sun orientation is perpendicular to the solar sail, then

$$a_c = \frac{2Pr_0 A_s}{m_0} = \frac{2Pr_0}{\sigma_T} \quad (2.6)$$

where $\sigma_T = \frac{m_0}{A_s}$ is mass to area ratio of the sail and m_0 is the total mass which is the

sum of payload mass and structural mass of the solar sail.

$$m_0 = m_{pl} + m_s$$

$$a_c = \frac{2Pr_0 A_s}{m_{pl} + m_s}$$

$$\Rightarrow A_s = \frac{m_{pl}}{\frac{2Pr_0}{a_c} - \sigma_s}$$

$$\sigma_s = \frac{m_s}{A_s}$$

Here σ_s is the sail assembly loading. It consists of the mass of the sail film and other structural mass. For a 100m x 100m sail, the assembly loading is estimated to be 10-14 g/m² [1]. For the f Figure 4, σ_s is taken as 10g/m² [5]. The solar sail acceleration at any distance from the sun is

$$a_{ss} = a_c \left(\frac{R_E}{r} \right)^2 \cos^2 \alpha \quad (2.7)$$

The characteristic acceleration depends upon the sail assembly loading, pitch angle and exposed surface area of the sail. For different characteristic accelerations, a square sail payload versus sail size relationship is shown in Figure 4.

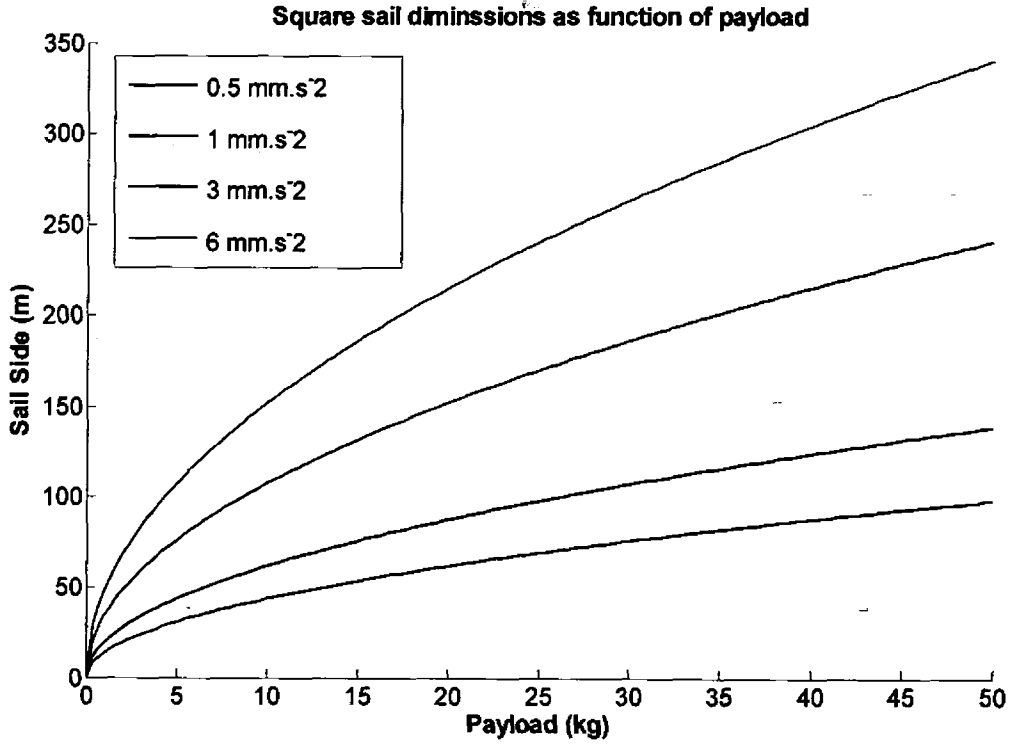


Figure 4- Payload Variation With Sail Area

The second performance parameter is the sail lightness number β_0 . It is the ratio of the sail acceleration, when it is normal to the sun, and the sun's gravitational acceleration.

$$\beta_0 = \frac{a_c \left(\frac{R_E}{r} \right)^2}{GM_s / r^2}$$

When $r = R_E$

$$\beta_0 = \frac{a_c R_E^2}{GM_s} = \frac{a_c}{5.93 \text{ mm/s}^2}$$

$$\beta_0 = \frac{2Pr_0 / \sigma_T}{5.93} = \frac{\sigma^*}{\sigma_T}$$

where $\sigma^* = \frac{2Pr_0}{5.93} = 1.53 \times 10^{-3} \text{ kg/m}^2$.

2.3.2 Non-Perfect reflecting solar sail

A perfect solar sail is an idealized model. Since a real sail is not a perfect reflector, therefore, for a real solar sail model reflection, absorption, transmission and emission coefficients are considered.

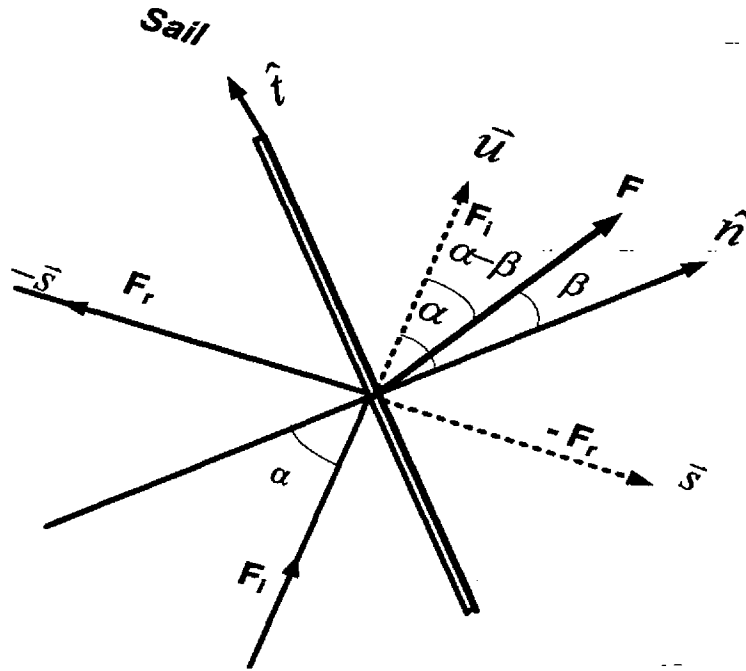


Figure 5– Non-perfect Reflecting Solar Sail

If the assumption of perfect reflectivity is relaxed, a more exact model for the solar radiation pressure force may be modeled [5].

$$\vec{F} = \vec{F}_a - \vec{F}_r + \vec{F}_e$$

$$\tilde{r} + \tilde{a} + \tilde{t} = 1$$

$$\tilde{r} + \tilde{a} = 1 \Rightarrow \tilde{a} = 1 - \tilde{r}$$

$$\vec{u} = \cos \alpha \hat{n} + \sin \alpha \hat{t}$$

$$\vec{s} = \cos \alpha \hat{n} - \sin \alpha \hat{t}$$

Here \vec{F}_r is the force due to perfect reflection, \vec{F}_a is the force due to absorption of photons and \vec{F}_e is the force due to emission by re-radiation, such that the fraction of absorption, reflection and emission has coefficients

$$\tilde{r} + \tilde{a} + \tilde{\tau} = 1$$

Supposing $\tilde{\tau} = 0$ on the reflective side of the solar sail, then

$$\tilde{r} + \tilde{a} = 1 \Rightarrow \tilde{a} = 1 - \tilde{r}$$

Now,

$$\vec{u} + \vec{s} = 2 \cos \alpha \hat{n}$$

Or
$$\vec{s} = -\vec{u} + 2 \cos \alpha \hat{n}$$

The force exerted by the absorbed photons on the solar sail is

$$\vec{F}_a = \text{Pr } A \cos \alpha \vec{u}$$

Or

$$\vec{F}_a = \text{Pr } A \cos \alpha (\cos \alpha \hat{n} + \sin \alpha \hat{t})$$

$$\vec{F}_a = \text{Pr } A (\cos^2 \alpha \hat{n} + \cos \alpha \sin \alpha \hat{t})$$

A fraction \tilde{r} of incident photon is reflected and another fraction of photons \tilde{s} is specularly reflected in the direction $-\vec{s}$, provides a force \vec{f}_{rs} in \vec{s} direction

$$\vec{f}_{rs} = (\tilde{r} \tilde{s}) \text{Pr } A \cos \alpha \vec{s}$$

In addition, another fraction of photons will be uniformly scattered from the reflecting surface of the sail due to non-specular reflection. This component will generate a force \vec{f}_{ru} in \hat{n} direction given by

$$\vec{f}_{ru} = B_f \tilde{r} (1 - \tilde{s}) \text{Pr } A \cos \alpha \hat{n}$$

where B_f is coefficient of non-Lambertian surface (A Lambertian surface is that which appears equally bright when viewed from any aspect angle). Therefore the total force due to reflected photons is given as

$$\vec{F}_r = \vec{f}_{rs} + \vec{f}_{ru}$$

Or writing the total force in terms of normal and transverse directions

$$\vec{F}_r = \text{Pr } A[(\tilde{r} \tilde{s} \cos^2 \alpha + B_f(1 - \tilde{s})\tilde{r} \cos \alpha)\hat{n} - \tilde{r} \tilde{s} \cos \alpha \sin \alpha \hat{t}]$$

The third component is due to those photons which have been absorbed and re-emitted from both front and rear surfaces of the sail. Since the power emitted from the unit area at temperature T is $\varepsilon\sigma T^4$, where ε is emissivity coefficient and σ is Boltzmann constant, therefore, the force due to emission by re-radiation is given as

$$\vec{F}_e = \frac{\sigma T^4}{c} (\varepsilon_f B_f - \varepsilon_b B_b) \hat{n}$$

where ε_f and ε_b are the front and back emissivity coefficients. The sail temperature can be obtained by using thermal input and thermal output in the solar sail

$$T = \left[\frac{(1 - \tilde{r})c \text{Pr} \cos \alpha}{\sigma(\varepsilon_f + \varepsilon_b)} \right]^{1/4}$$

Thus, the force exerted on the solar sail due to emission by re-radiation is

$$\vec{F}_e = \text{Pr } A(1 - \tilde{r}) \frac{\varepsilon_f B_f - \varepsilon_b B_b}{\varepsilon_f + \varepsilon_b} \cos \alpha \hat{n}$$

It is clear that this force is maximized by a larger value of ε_f and a smaller value of ε_b .

Combining all these three components, the total force exerted on the sail can be written in terms of normal and transverse components as

$$\vec{F}_n = \text{Pr } A \left\{ \begin{array}{l} (1 + \tilde{r} \tilde{s}) \cos^2 \alpha + B_f(1 - \tilde{s})\tilde{r} \cos \alpha \\ + (1 - \tilde{r}) \frac{\varepsilon_f B_f - \varepsilon_b B_b}{\varepsilon_f + \varepsilon_b} \cos \alpha \end{array} \right\} \hat{n} \quad (2.8)$$

$$\vec{F}_t = Pr A(1 - \hat{r}\tilde{s}) \cos \alpha \sin \alpha \hat{t} \quad (2.9)$$

Bernd Dachwald gives, in Ref. [12], values of optical coefficients for a sail with a highly reflective aluminum coated front side and highly emissive chromium coated back side. These values are given in the following table:

Table 1- Optical Coefficients for an Al/Cr Coated Sail

Parameters	Front side	Back side
	(Aluminum Coated)	(Chromium Coated)
\tilde{r}	0.88	
\tilde{s}	0.94	
\mathcal{E}	0.05	0.55
B	0.79	0.55

The magnitude of total force on a non-perfect solar sail due solar SRP is then calculated as

$$F = \sqrt{F_n^2 + F_t^2} \quad (2.10)$$

Since the sail is non-perfect reflector, the direction of this force is along the normal to the sail. The angle β , between the force vector and the sail normal is a centre line angle, is defined as

$$\beta = \tan^{-1} \left[\frac{F_t}{F_n} \right] \quad (2.11)$$

Magnitudes of normal and transverse components of the force and total force verses pitch angle of the sail by using the data of a sail in Table 1, are shown in Figure 6.

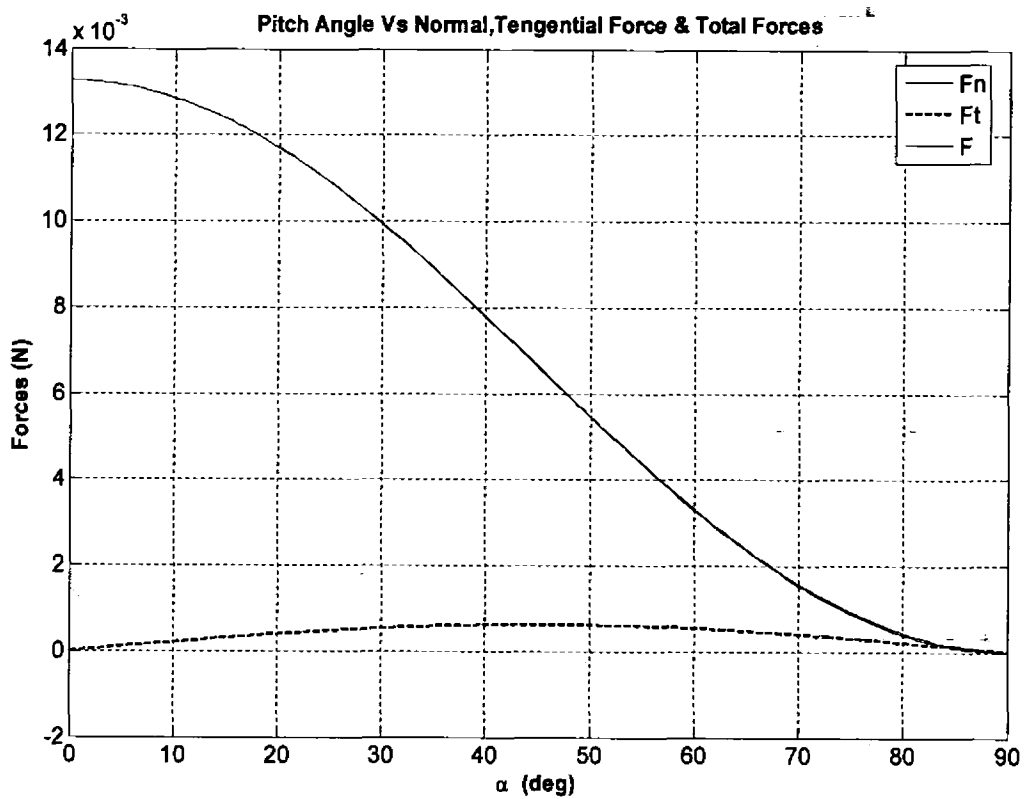


Figure 6 - SRP Force Varies With Pitch Angle of Sail

Chapter 3

3. Fundamentals of Attitude Dynamics

The formulation of interplanetary spacecraft and satellite attitude dynamics and control problems involves considerations of both kinematics and dynamics. In this chapter, the rotational kinematics and dynamics of a satellite, under a rigid body assumption, will be described.

3.1 Rotational Kinematics

In kinematics, we are primarily interested in describing the orientation of a body during its rotational motion. Rotational kinematics does not involve any associated forces. It is convenient to describe the orientation of a satellite or spacecraft with respect to some fixed inertial frame by using some generalized coordinates. Direction cosines are not generalized coordinates, since they are not independent, but are related by a constraint. A set of generalized coordinates that may be selected to describe the orientation of satellite consists of Euler angles ([13] & [14]) Rodrigues Parameters, Modified Rodrigues Parameters ([18],[19],& [20]) or quaternion.

3.1.1 Euler Angles

A scheme to align a rigid body with the desired orientation is called body axis rotation. It involves three successive rotations about the axes of the rotated, body-fixed reference frame. The first rotation is about any axis. The second rotation is about either of the two axes not used for the first rotation. The third rotation is then about either of the two axes not used in the second rotation. The choice of Euler angles is not unique but they involve three successive angular displacements for the transformation from a set of Cartesian coordinates to another. The rotations are not about three orthogonal axes. The three components of angular velocity of a satellite can be expressed in terms of Euler angles and their time derivatives.

In Fig. 7, the rectangular frame B is assumed to be a body coordinate system with a right-handed set of three unit orthogonal vectors $[\hat{b}_1, \hat{b}_2, \hat{b}_3]$. We are interested in

describing the location of the body frame with respect to the reference frame A, having a right-handed set of three orthogonal vectors $[\hat{a}_1, \hat{a}_2, \hat{a}_3]$. A sequence of rotations is used for the A frame in order that it coincides with the B frame. Let these rotations be yaw ψ , pitch θ and roll ϕ . These angles are called Euler angles ([2] & [14]).

Consider the rotational sequence of $C_1(\phi) \leftarrow C_2(\theta) \leftarrow C_3(\psi)$ which are symbolically represented as

$$C_3(\psi): A' \rightarrow A$$

$$C_2(\theta): A'' \rightarrow A'$$

$$C_1(\phi): A''' \rightarrow A''$$

Then the angular velocity vector $\bar{\omega}$ of the satellite is given in Equation (3.1).

$$\bar{\omega} = \dot{\psi} \hat{b}_3 + \dot{\theta} \hat{j}_a + \dot{\phi} \hat{a}_1 \quad (3.1)$$

where \hat{j}_a is an intermediate axis of rotation.

If $C_1(\phi)$, $C_2(\theta)$ and $C_3(\psi)$ be the direction cosine matrices of rotations,

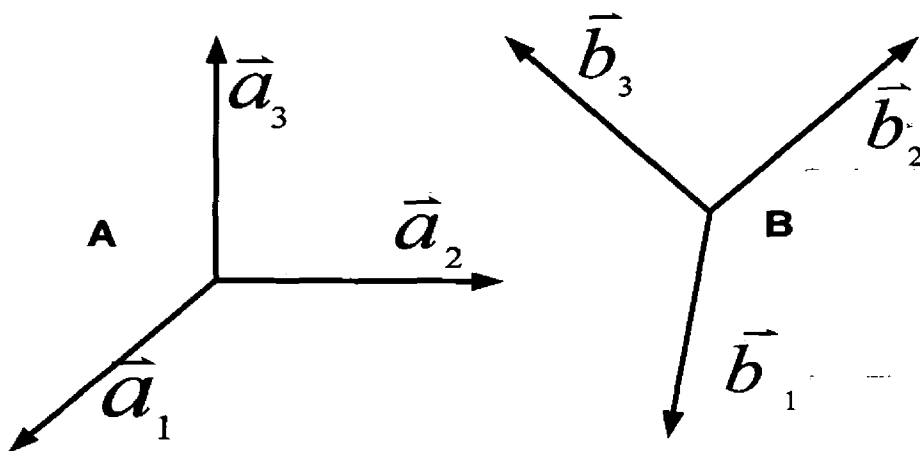


Figure 7 - Euler Angles

then equations (3.1) can be written as

$$\begin{bmatrix} \omega_1 \\ \omega_2 \\ \omega_3 \end{bmatrix} = \begin{bmatrix} \dot{\phi} \\ 0 \\ 0 \end{bmatrix} + C_1(\phi) \begin{bmatrix} 0 \\ \dot{\theta} \\ 0 \end{bmatrix} + C_1(\phi)C_2(\theta) \begin{bmatrix} 0 \\ 0 \\ \dot{\psi} \end{bmatrix} \quad (3.2)$$

The direction cosine matrices are given as

$$C_1(\phi) = \begin{pmatrix} 1 & 0 & 0 \\ 0 & \cos(\phi) & \sin(\phi) \\ 0 & -\sin(\phi) & \cos(\phi) \end{pmatrix}$$

$$C_2(\theta) = \begin{pmatrix} \cos(\theta) & 0 & -\sin(\theta) \\ 0 & 1 & 0 \\ \sin(\theta) & 0 & \cos(\theta) \end{pmatrix}$$

$$C_3(\psi) = \begin{pmatrix} \cos(\psi) & \sin(\psi) & 0 \\ -\sin(\psi) & \cos(\psi) & 0 \\ 0 & 0 & 1 \end{pmatrix}$$

Using all the above three transformation matrices in equation (3.2), we get the angular velocity vector in body frame as

$$\begin{bmatrix} \omega_1 \\ \omega_2 \\ \omega_3 \end{bmatrix} = \begin{pmatrix} 1 & 0 & -\sin(\theta) \\ 0 & \cos(\phi) & \sin(\phi)\cos(\theta) \\ 0 & -\sin(\phi) & \cos(\phi)\cos(\theta) \end{pmatrix} \begin{bmatrix} \dot{\phi} \\ \dot{\theta} \\ \dot{\psi} \end{bmatrix} \quad (3.3)$$

By taking inverse of the coefficient matrix, the last equation becomes

$$\dot{\bar{\Phi}} = S(\bar{\Phi})\bar{\omega} \quad (3.4)$$

Equations (3.4) are the kinematic equations of the satellite. Here,

$$\bar{\Phi} = \begin{bmatrix} \phi \\ \theta \\ \psi \end{bmatrix} \quad \text{and} \quad S(\bar{\Phi}) = \frac{1}{\cos(\theta)} \begin{pmatrix} \cos(\theta) & \sin(\phi)\sin(\theta) & \cos(\phi)\sin(\theta) \\ 0 & \cos(\phi)\cos(\theta) & -\sin(\phi)\cos(\theta) \\ 0 & \sin(\phi) & \cos(\phi) \end{pmatrix}$$

Note that the equations (3.4) are not defined when $\cos(\theta)$ becomes zero. It is a singularity for this sequence of Euler angles. For other sequences such singularities occur for other angles. To overcome this problem, they are rewritten by using Quaternion representation.

3.1.2 Quaternion Representation

The Euler angles are actually rotations about three different axes. The orientation can be described by a single rotation about some reference axis $\{\hat{k}\}$ by an angle θ_1 . This is done by using unit quaternion \bar{q} having four components [14]

$$\bar{q} = \begin{bmatrix} q_1 \\ q_2 \\ q_3 \\ q_4 \end{bmatrix}$$

These components are defined as

$$\begin{aligned} q_4 &= \cos\left(\frac{\theta_1}{2}\right) & ; & & q_1 &= k_x \sin\left(\frac{\theta_1}{2}\right) \\ q_2 &= k_y \sin\left(\frac{\theta_1}{2}\right) & ; & & q_3 &= k_z \sin\left(\frac{\theta_1}{2}\right) \end{aligned}$$

Conversion from Euler angles to quaternion is given by following relations

$$\begin{aligned} q_1 &= \sin(\phi/2)\cos(\theta/2)\cos(\psi/2) - \cos(\phi/2)\sin(\theta/2)\sin(\psi/2) \\ q_2 &= \cos(\phi/2)\sin(\theta/2)\cos(\psi/2) + \sin(\phi/2)\cos(\theta/2)\sin(\psi/2) \\ q_3 &= \cos(\phi/2)\cos(\theta/2)\sin(\psi/2) - \sin(\phi/2)\sin(\theta/2)\cos(\psi/2) \\ q_4 &= \cos(\phi/2)\cos(\theta/2)\cos(\psi/2) + \sin(\phi/2)\sin(\theta/2)\sin(\psi/2) \end{aligned}$$

Differentiating the above set of equations with respect to time, we get

$$\dot{\bar{q}} = \frac{1}{2} T(\bar{\Phi}) \dot{\bar{\Phi}} \quad (3.5)$$

where the value of $T(\bar{\Phi})$ is given in Equation (3.7). Putting the value of $\dot{\bar{\Phi}}$ from Equation (3.4) in Equation (3.5), we get

$$\dot{\bar{q}} = \frac{1}{2} T(\bar{\Phi}) S(\bar{\Phi}) \bar{\omega} \quad (3.6)$$

$$T(\bar{\Phi}) S(\bar{\Phi}) = \begin{bmatrix} q_4 & -q_3 & q_2 & q_1 \\ q_3 & q_4 & -q_1 & q_2 \\ -q_2 & q_1 & q_4 & q_3 \\ -q_1 & -q_2 & -q_3 & q_4 \end{bmatrix} \quad (3.7)$$

Equation (3.6) can be further simplified as

$$\dot{\bar{q}} = \frac{1}{2} G(\bar{q}) \bar{\omega} \quad (3.8)$$

where

$$G(\bar{q}) = T(\bar{\Phi}) S(\bar{\Phi}) \quad (3.9)$$

Equations (3.8) are the kinematic equations of the satellite in quaternion form.

3.1.3 Modified Rodrigues Parameters

Modified Rodrigues Parameters (MRPs) are used to describe the kinematic equations of a spacecraft. This parameterization is derived by applying a stereographic projection of the quaternion. Since the quaternion representation is given by

$$\bar{q} = \begin{bmatrix} q_1 \\ q_2 \\ q_3 \\ q_4 \end{bmatrix}$$

$$\bar{q} = \begin{bmatrix} \bar{q}_{13} \\ \text{---} \\ q_4 \end{bmatrix}$$

$$\bar{q}_{13} = \begin{bmatrix} q_1 \\ q_2 \\ q_3 \end{bmatrix} = \hat{k} \sin(\theta_1 / 2)$$

$$q_4 = \cos(\theta_1 / 2)$$

where \hat{k} is a unit vector corresponding to the axis of rotation and θ_1 is the angle of rotation. The Modified Rodrigues parameters are defined as

$$\bar{p} = \begin{bmatrix} p_1 \\ p_2 \\ p_3 \end{bmatrix} = \frac{\bar{q}_{13}}{1 + q_4} \quad (3.10)$$

The kinematic equation of motion are derived by using the spacecraft angular velocity are given by

$$\dot{\bar{p}} = \frac{1}{4} \{ (1 - \bar{p}^T \bar{p}) I_{3 \times 3} + 2[p^\times] + 2\bar{p}\bar{p}^T \} \bar{\omega} \quad (3.11)$$

where $[p^\times]$ is a cross product matrix defined by

$$[p^\times] = \begin{bmatrix} 0 & -p_3 & p_2 \\ p_3 & 0 & -p_1 \\ -p_2 & p_1 & 0 \end{bmatrix}$$

3.2 Rigid-Body Dynamics

In this section, satellite dynamics literature is reviewed and some basic properties of satellite dynamics are established ([2] & [4]). Assume the satellite to be a rigid body

with mass center B^* as shown in Figure 8. Reference frame B is fixed in the body. Given the element of mass ' dm ' whose location relative to B^* is

$$\vec{r} = r_1 \vec{b}_1 + r_2 \vec{b}_2 + r_3 \vec{b}_3 \quad (3.12)$$

The moment of inertia matrix is defined by

$$I = \begin{pmatrix} I_{11} & I_{12} & I_{13} \\ I_{21} & I_{22} & I_{23} \\ I_{31} & I_{32} & I_{33} \end{pmatrix}$$

where

$$I_{11} = \int_B (r_2^2 + r_3^2) dm$$

$$I_{22} = \int_B (r_1^2 + r_3^2) dm$$

$$I_{33} = \int_B (r_1^2 + r_2^2) dm$$

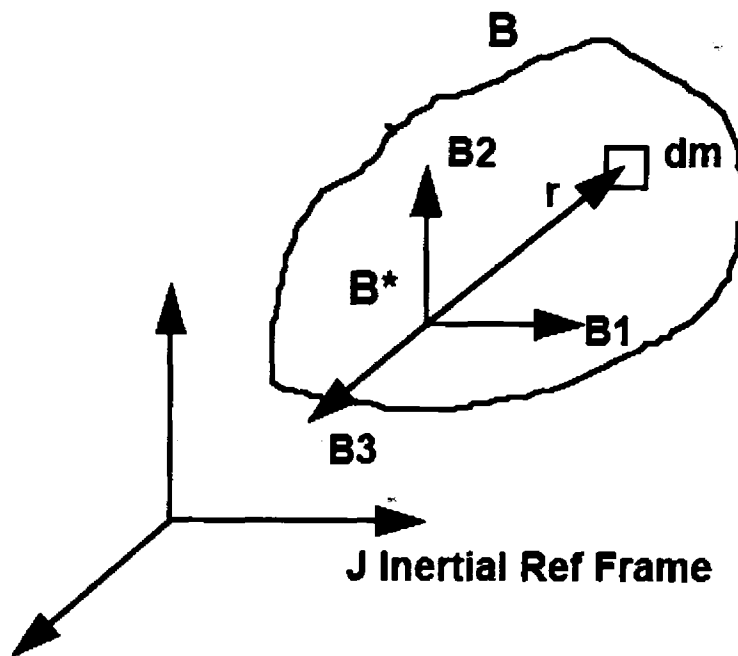


Figure 8- Reference Frame and Mass Element and the non-diagonal elements are given by the relation

7A-8474

$$I_{ij} = - \int_B r_i r_j dm, \quad i \neq j$$

Note that I is a symmetric matrix. If $\bar{\omega}$ is the angular velocity vector of the rigid body, then its angular momentum \bar{H} is given by the following relation

$$\bar{H} = I\bar{\omega} \quad (3.13)$$

$$H_1 = I_{11}\omega_1 + I_{12}\omega_2 + I_{13}\omega_3$$

$$H_2 = I_{21}\omega_1 + I_{22}\omega_2 + I_{23}\omega_3$$

$$H_3 = I_{31}\omega_1 + I_{32}\omega_2 + I_{33}\omega_3$$

The rotational kinetic energy is

$$E_k = \frac{1}{2} \bar{\omega}^T \bar{H} = \frac{1}{2} \bar{\omega}^T I \bar{\omega} = \frac{1}{2} \sum_{i=1}^3 \sum_{j=1}^3 I_{ij} \omega_i \omega_j \quad (3.14)$$

The equations of motion are:

$$\frac{d\bar{H}}{dt} = \bar{T} \quad (3.15)$$

where \bar{T} is the net torque acting on the body. By taking derivative of the angular momentum given by Equation (3.13), we get

$$\frac{d\bar{H}}{dt} = I\dot{\bar{\omega}} + \bar{\omega} \times I\bar{\omega} = \bar{T} \quad (3.16)$$

These equations have been derived for a rigid body but they can be applied to any system of particles and/or rigid bodies as long as the torques are computed about the reference point. We take center of mass of the system as our reference point for the angular momentum. If the axes are the principal axes then the inertia matrix becomes a diagonal matrix and the equations of motion become

$$\left. \begin{aligned} I_{11}\dot{\omega}_1 + \omega_2\omega_3(I_{33} - I_{22}) &= T_1 \\ I_{22}\dot{\omega}_2 + \omega_1\omega_3(I_{11} - I_{33}) &= T_2 \\ I_{33}\dot{\omega}_3 + \omega_1\omega_2(I_{22} - I_{11}) &= T_3 \end{aligned} \right\} \quad (3.17)$$

These are called Euler's equations of motion for a rigid body.

3.2.1 Spin Stabilization of Solar Sail Spacecraft

A simple solution to the problem of maintaining a desired orientation of a sail craft in the presence of a cm (centre of mass of the solar sail) and cp (centre of solar radiation pressure of the solar sail) offset is to spin the sail craft about its roll axis. A thrust vector misalignment with the roll axis caused by a cm/cp offset will cause the sail craft to tumble in the absence of spinning or active three-axis control. However, a spinning sail craft possesses a gyroscopic stiffness to external disturbances, and its motion under the influence of external disturbances is characterized by the precession and nutation of the roll axis about the desired direction of the roll axis [4]. The orientation of a spinning sail craft can be changed by precession of the sail craft using thrusters. Three axis attitude control of a square solar sail can be achieved by several ways. One of these methods is to use control boom and vanes structure to displace the centre of mass relative to the centre of pressure of the sail. This can be achieved by mounting the payload on an articulated boom and utilizing boom rotations to control the centre of mass location. This architecture provides an effective precession control torque to a spinning sail craft with a large angular momentum. For the purpose of studying the effect of a cm/cp off set on a spinning sail craft, consider a sail craft possessing a body fixed frame B with basis $[\bar{b}_1, \bar{b}_2, \bar{b}_3]$ vectors and with its origin at the center of mass. Let the reference frame B coincides with principal axes. It is assumed that the 1st axis is the roll (spin) axis perpendicular to the sail surface and the 2nd and 3rd axes are the pitch/yaw (transverse) axes. The solar pressure force vector is nominally aligned along \bar{b}_1 through the center of pressure of the sail craft. Euler's rotational equations of motion of a rigid sail craft are given by

$$\left. \begin{aligned} I_{11}\dot{\omega}_1 + \omega_2\omega_3(I_{33} - I_{22}) &= T_1 \\ I_{22}\dot{\omega}_2 + \omega_1\omega_3(I_{11} - I_{33}) &= T_2 \\ I_{33}\dot{\omega}_3 + \omega_1\omega_2(I_{22} - I_{11}) &= T_3 \end{aligned} \right\}$$

For a square sail craft, let $I_{22} = I_{33} = I$ then the rotational equations become

$$\left. \begin{aligned} I_{11}\dot{\omega}_1 &= 0 \\ I\dot{\omega}_2 - \omega_1\omega_3(I - I_{11}) &= T_2 \\ I\dot{\omega}_3 - \omega_1\omega_2(I_{11} - I) &= T_3 \end{aligned} \right\} \quad (3.18)$$

where T_2 and T_3 are the solar pressure torque vector components due to centre of mass and centre of pressure offset. From first of the equations (3.18) we have

$$\omega_1 = \text{constant} = \Omega \quad (3.23)$$

For simplicity, let us suppose that pitch/yaw axes are chosen such that $T_2 = 0$ and $T_3 = \varepsilon F$ where ε is a cm/cp offset distance and \vec{F} is solar radiation pressure force.

Thus, the last two equations (3.22) becomes

$$\left. \begin{aligned} \dot{\omega}_2 &= -\lambda \omega_3 \\ \dot{\omega}_3 &= \lambda \omega_2 + \mu \end{aligned} \right\} \quad (3.19)$$

where $\lambda = \Omega(I_1 - I)/I$ and the disturbance acceleration $\mu = \varepsilon F/I$ is due to the offset of cm/cp. We can describe the rotational motion of the spinning sail craft, as seen from an inertial reference frame, as a body-fixed rotational sequence of roll(ϕ), pitch(θ) and yaw(ψ). For this rotational sequence, we have the following kinematic differential equations

$$\left. \begin{aligned} \dot{\phi} &= \omega_1 + (\omega_2 \sin \phi + \omega_3 \cos \phi) \tan \theta \\ \dot{\theta} &= \omega_2 \cos \phi - \omega_3 \sin \phi \\ \dot{\psi} &= (\omega_2 \sin \phi + \omega_3 \cos \phi) / \cos \theta \end{aligned} \right\} \quad (3.20)$$

The system of coupled non-linear equations (3.17) and (3.20) has been simultaneously solved, numerically, by using some appropriate ordinary differential equation (ODE) solver in MATLAB. The code is given in the appendix. Simulation results for a 40m×40m sail craft with a spin axis angular velocity of 0.5deg/s and all other initial conditions set to zero, having the following parameter values, are shown in Figure 10.

Table 2- Sail Characteristics

Parameter	I_1	$I_2 = I_3$	Ω	F	ϵ
Value	6000 kg-m ²	3000 kg-m ²	0.5 deg/s	0.01 N	0.1 m

This non-linear simulation result is in agreement with the linear analysis results presented in Ref.[5]. The subplot (2,2) in Figure 10 shows the path of the tip of the roll axis in space.

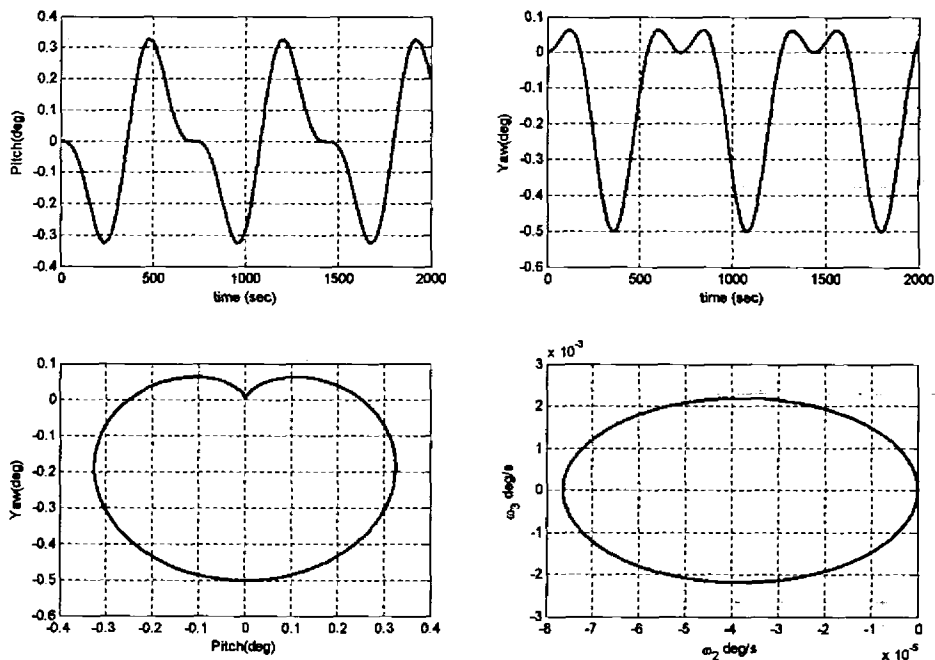


Figure 9 - Simulation Results for a cm/cp 0.1 m offset

Rigid body dynamics is a dynamical system with, in general, six degrees of freedom. Three degrees of freedom are associated with the translational motion while the other three are associated with the rotational motion. The spacecraft is considered to be a rigid body whose attitude can be described by two sets of equations. The dynamic equations given in Equ.(3.17) are coupled, non-linear and first order differential equations. When these equations are solved, we get the angular velocity components of the rigid body, no information is attained about the orientation of the body. So, we need the kinematic equations, given in Equ (3.20), to specify the orientation of the

body. The kinematic equations incorporate the angular velocity components from dynamic equations and the Euler angles ϕ, θ, ψ in the body frame. For the orientation of the spacecraft, we use various parameterizations. Attitude representations can be done using three or four parameters. The three parameters attitude representation techniques are Euler angles, Cayley Rodrigues Vector or Modified Rodrigues Parameters (MRPs). The four parameter representation is in the form of quaternions. All these representations have their own advantages and disadvantages. For example, in Euler angle representation, the Jacobian matrix in the kinematic equations has singularities. The unit quaternion, globally represent the spacecraft attitude without singularities. But in this presentation an additional constraint equation is introduced which leads to non-minimal parameterization. Here, for one of our control scheme we use Euler angle parameterization and for the other one Modified Rodrigues Parameters (MRPs) are used. The advantage of MRPs is that we can perform extremely large rotations (up to 360°) while using minimal parameterization.

3.2.2 Rotational Control Torques Generation Using Control Boom and Control Vans

Three axis attitude control of a square solar sail may be accomplished by several means. One method is to displace the centre of mass of the solar sail with respect to the centre of pressure [4]. This cm/cp offset can be achieved by various methods [15]. One of these methods is to mount the payload on a gimbaled boom and utilizing boom rotations to control the centre of mass location. An alternative method of three-axis attitude control is the use of the spars tip-mounted vanes. The tip vanes are small reflective panels attached to the ends of the spars through drive motors. Although the forces generated by a tip vane are small but the large moment arm relative to the centre of mass of the sail can provide suitable control torques [5]. A better control authority can be achieved through the combination of both these methods. The architecture of a hybrid control method for a square sail is shown in Figure 2.

Consider an ideal flat solar sail with body axes (x,y,z) as shown in Figure 2. Yaw, pitch and roll rotations are defined about x-axis, y-axis and z-axis, respectively. Let

m_p be located at the end of the boom of fixed length l so that the position of the payload defined in the body axes is

$$\bar{\mathbf{r}}_p = l \cos \nu \cos \chi \hat{e}_1 + l \cos \nu \sin \chi \hat{e}_2 + l \sin \nu \hat{e}_3 \quad (3.21)$$

Where ν is the boom elevation angle and χ is the boom azimuth relative to the solar sail body axes and \hat{e}_1 , \hat{e}_2 and \hat{e}_3 are shown in Figure 2. If mass of the solar sail, excluding the payload mass, is m_s then the position of the centre of mass $\bar{\mathbf{r}}_c$ is defined in body axes as

$$\bar{\mathbf{r}}_c = \frac{m_p}{m_p + m_s} \bar{\mathbf{r}}_p \quad (3.22)$$

Since length of boom is fixed, the centre of mass location can be displaced on the surface of hemispherical radius $m_p / (m_p + m_s)$ of the sunward face of the sail. For an ideal sail, the force exerted by the solar radiation as given in Equ. (2.5) is

$$\bar{\mathbf{F}} = F_s (\hat{\mathbf{S}} \cdot \hat{\mathbf{n}})^2 \hat{\mathbf{n}} \quad (3.23)$$

where $\hat{\mathbf{S}}$ is a vector from the Sun to the sail surface and $\hat{\mathbf{n}}$ is unit vector normal to the sail surface. Therefore, the vector equation of the torque exerted is

$$\bar{\mathbf{T}} = -\bar{\mathbf{r}}_c \times \bar{\mathbf{F}} = -\left(\frac{m_p}{m_p + m_s}\right) \bar{\mathbf{r}}_p \times \bar{\mathbf{F}}$$

The scalar form of the equation is

$$\left. \begin{aligned}
 T_1 &= -F_s \left(\frac{m_p}{m_p + m_s} \right) l \cos^2 \alpha \cos \nu \cos \chi \\
 T_2 &= -F_s \left(\frac{m_p}{m_p + m_s} \right) l \cos^2 \alpha \cos \nu \sin \chi \\
 T_3 &= 0
 \end{aligned} \right\} \quad (3.24)$$

where T_1 is yaw torque, T_2 is pitch torque and T_3 is roll torque. When the sail is flat and ideal then T_3 is zero but in case of non-ideal sail there is small roll torque. It can be seen that the magnitude of the torque can be controlled using the elevation angle and the length of the boom while the direction of the torque can be controlled via the boom azimuth. For an ideal solar sail in Sun-facing attitude, pitch and yaw torques are shown in Figure 11 and Figure 12.

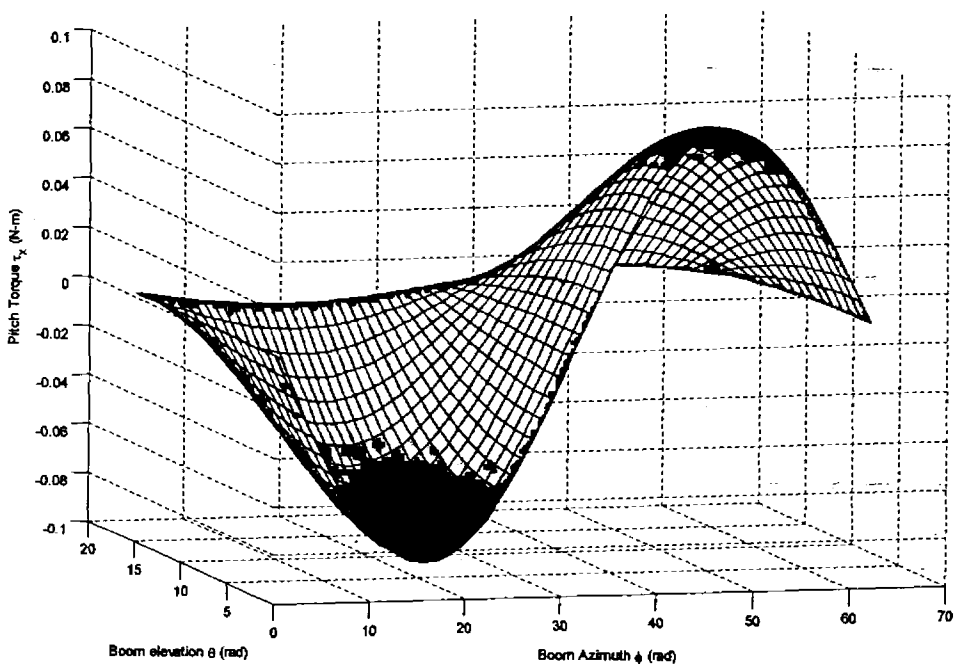


Figure 10- Pitch Torque as a Function of Elevation and Azimuth

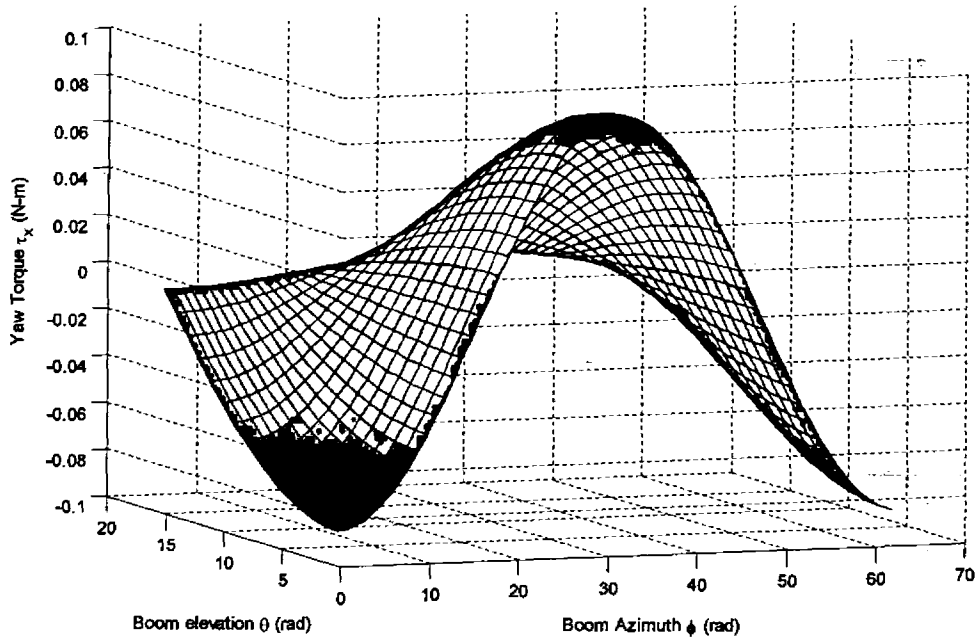


Figure 11 - Yaw Torque as a Function of Elevation and Azimuth

For three axes control, tip vanes are used. Let us consider a square sail having two tip vanes at the ends of the x-axis of the sail as shown in Figure 2 . These vanes provide only pitch and roll torques but yaw torque can also be obtained by a combination of both pitch and roll torques.

It is assumed that the vanes may only be rotated about the spar axis through a clockwise rotation delta. The unit normal vector to each vane may be written in solar sail body axis as

$$\begin{aligned}\hat{n}_1 &= \sin \delta_1 \hat{e}_2 - \cos \delta_1 \hat{e}_3 \\ \hat{n}_2 &= -\sin \delta_2 \hat{e}_2 - \cos \delta_2 \hat{e}_3\end{aligned}$$

The components of these unit vectors are in y-z plane under above assumption. This is shown in Figure 12(a), and Figure 12(b).

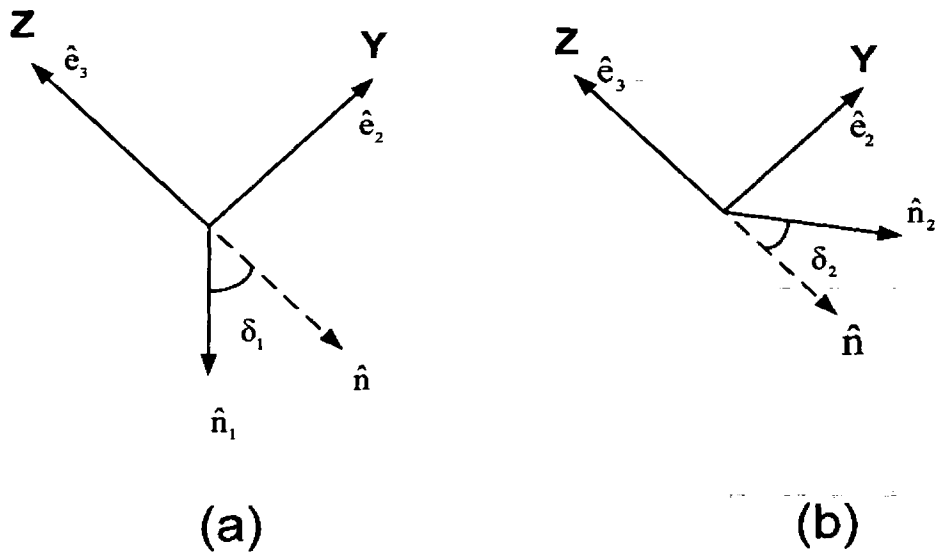


Figure 12 - Two Vans Orientation

Let us make another assumption, for our ease, that the sun line is in x-z plane and α is the angle from sun line to z-axis as illustrated in Figure 13.

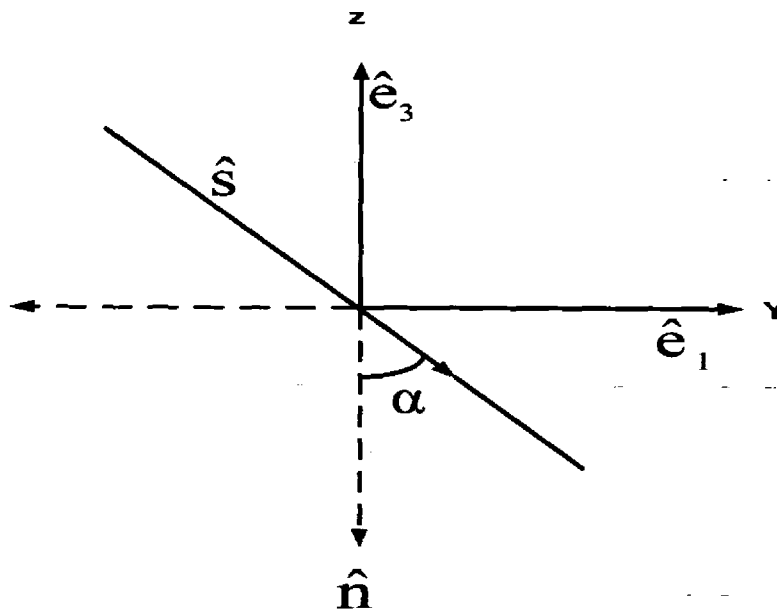


Figure 13- Sun Vector in Body Frame

The Sun vector \hat{S} in the sail body frame is expressed

$$\hat{S} = \sin(\alpha)\hat{e}_1 - \cos(\alpha)\hat{e}_3$$

For simplicity another assumption is made that the center of mass is the geometrical center of the sail and distance from each van center to the center of the sail is taken as d . Two vans are shown in Figure 2 along x-axis, there position vectors are

$$\left. \begin{aligned} \bar{d}_1 &= d \hat{e}_1 \\ \bar{d}_2 &= -d \hat{e}_1 \end{aligned} \right\}$$

From equation (3.23)

$$\bar{F} = F_s (\hat{s} \cdot \hat{n})^2 \hat{n}$$

The torque which provides control from i^{th} vane is

$$\bar{T}_i = \bar{d}_i \times F_s (\hat{s} \cdot \hat{n}_i)^2 \hat{n}_i$$

where d_i is the location of i^{th} vane relative to the solar sail center of mass and F_s is the tip vane force obtained from the sun facing. In our case two vans are available, so the forces in body frame are

$$\left. \begin{aligned} \bar{F}_1 &= F_s \cos^2(\alpha) \cos^2(\delta_1) \sin(\delta_1) \hat{e}_2 - F_s \cos^2(\alpha) \cos^3(\delta_1) \hat{e}_3 \\ \bar{F}_2 &= -F_s \cos^2(\alpha) \cos^2(\delta_2) \sin(\delta_2) \hat{e}_2 - F_s \cos^2(\alpha) \cos^3(\delta_2) \hat{e}_3 \end{aligned} \right\}$$

and torques from the two vans are

$$\bar{T}_1 = \begin{vmatrix} \hat{e}_1 & \hat{e}_2 & \hat{e}_3 \\ d & 0 & 0 \\ 0 & F_s \cos^2(\alpha) \cos^2(\delta_1) \sin(\delta_1) & -F_s \cos^2(\alpha) \cos^3(\delta_1) \end{vmatrix}$$

$$\bar{T}_2 = \begin{vmatrix} \hat{e}_1 & \hat{e}_2 & \hat{e}_3 \\ d & 0 & 0 \\ 0 & -F_s \cos^2(\alpha) \cos^2(\delta_2) \sin(\delta_2) & -F_s \cos^2(\alpha) \cos^3(\delta_2) \end{vmatrix}$$

The component torque equations of combined torque $\bar{T} = \bar{T}_1 + \bar{T}_2$ from the both vans are then

$$\left. \begin{aligned} T_1 &= 0 \\ T_2 &= F_s d \cos^2 \alpha (\cos^3 \delta_1 - \cos^3 \delta_2) \\ T_3 &= F_s d \cos^2 \alpha (\cos^2 \delta_1 \sin \delta_1 - \cos^2 \delta_2 \sin \delta_2) \end{aligned} \right\} \quad (3.25)$$

Therefore, through appropriate combination of vane rotations, arbitrary pitch and roll torques may be generated. Roll torque is generated through a collective rotation of both vanes. Vane rotation angles and area of the tip vanes are used to generate the necessary maximum torque expected during the solar sail mission.

For an ideal solar sail in Sun-facing attitude, pitch and yaw torques are shown in Figure 13 and Figure 14. It can be seen that full control authority can be achieved in both pitch and roll. If only yaw control is required, then it can be demonstrated that full three axis control can in fact be obtained with only two vanes located at the tips of the x-axis spar. The sail is firstly rolled by 90 degree using collective rotation to two vanes and then the sail is pitched to the desired attitude. Finally, it is rolled back through 90 degree. This full sequence of rotation then corresponds to the change in the sail yaw attitude.

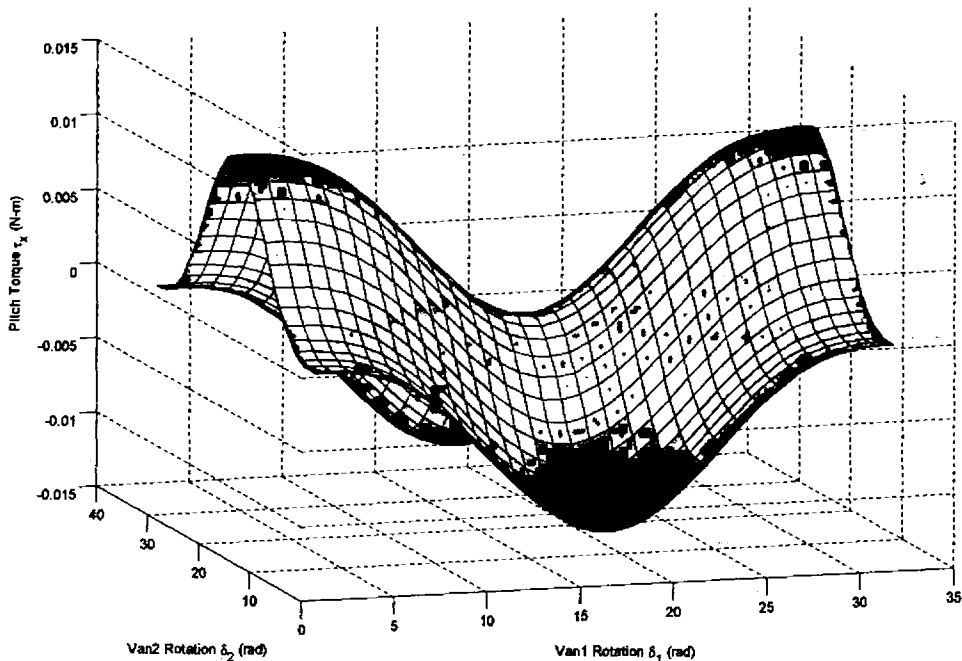


Figure 14 - Pitch Torque τ_x as a Function of Vane Rotations

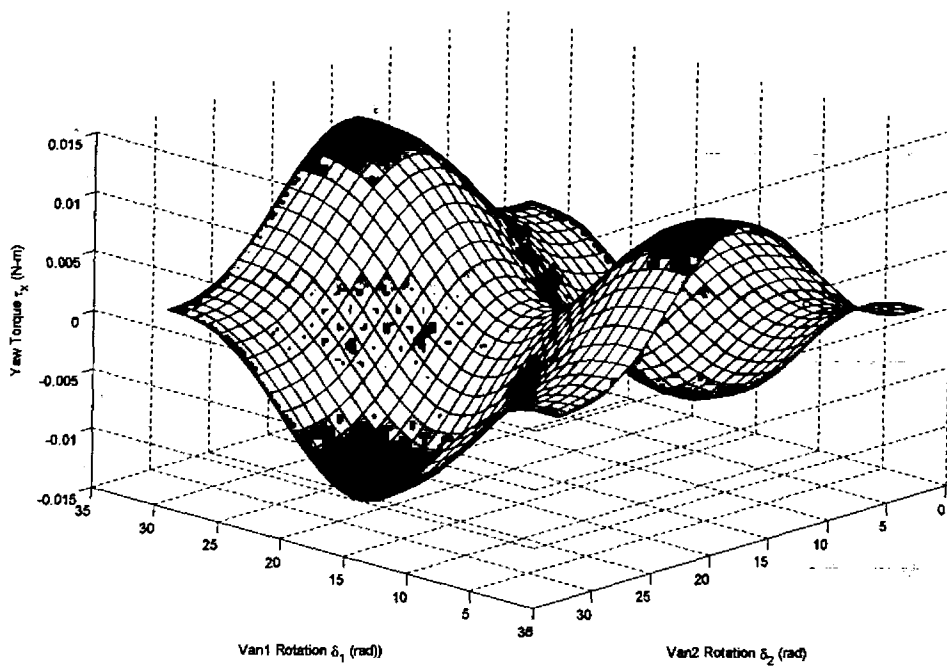


Figure 15 - Roll Torque as a Function of Vane Rotations

The tip vanes and centre of mass displacement have their own particular advantages and disadvantages for a solar sail attitude control [5]. In practice, combination of more than one method may provide the optimal solution for good three-axis attitude control.

Chapter 4

4. Attitude Controller Design

This chapter begins from where the chapter on rotational dynamics and kinematics is left off. Maximum absolute torque achieved from both control boom and control vanes mechanism has already been studied in the previous chapter. In this chapter, we are going to introduce two non-linear control schemes which are more suitable for our problem. The control of spacecraft for large angle slewing maneuvers and for small torques achieved from actuator mechanism makes the problem difficult. These difficulties include a highly non-linear characteristic of the governing equations, uncertainties in modeling and structure of the spacecraft, control rate and saturation constraints and limits and incomplete state knowledge due to sensor failures or omission. In our case we also have larger maneuvers, smaller thrust and smaller maneuvering torques. The main problem addressed in this chapter is the attitude tracking control. We can also use the controllers developed here for the regulation problem.

For our control problem, following controllers are described in details:

- State Feedback Controller
- Sliding Mode Controller

4.1 State Feedback Controller

The state feedback controller is developed on the basis of the dynamic and kinematic equations (3.17) and (3.20), respectively. The state vector $\bar{x} = [\omega_1, \omega_2, \omega_3, \phi, \theta, \psi]$ is taken as feedback to the controller. This controller is used for the tracking problem. The tracking error is considered as the difference between the current Euler angles and the desired Euler angles.

Non-linear proportional derivative control logic is considered as follows:

$$\left. \begin{aligned} T_1 &= -\text{sat}_U \left\{ k_1 (\phi - \phi_{ref}) + c_1 \omega_1 \right\} \\ T_2 &= -\text{sat}_U \left\{ k_2 (\theta - \theta_{ref}) + c_2 \omega_2 \right\} \\ T_3 &= -\text{sat}_U \left\{ k_3 (\psi - \psi_{ref}) + c_3 \omega_3 \right\} \end{aligned} \right\} \quad (4.1)$$

where $\bar{T} = [T_1, T_2, T_3]^T$ is the maximum control torque available in each axis and $\bar{K} = [k_1, k_2, k_3]^T$ and $\bar{C} = [c_1, c_2, c_3]^T$ are PD gains of the controller.

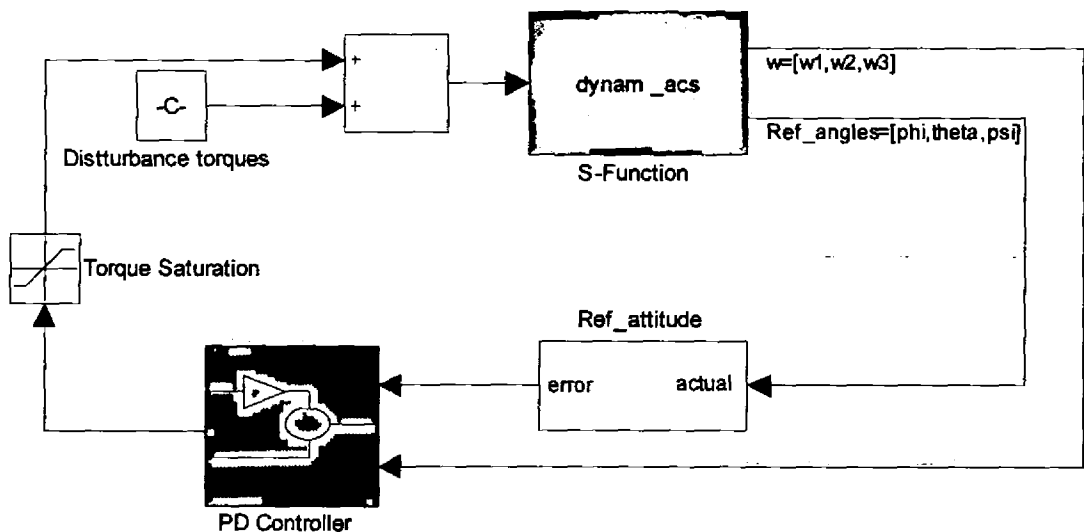


Figure 16: State feedback controller

4.2 Sliding Mode Controller

Modeling uncertainties have strong adverse effect on the non-linear control system. One of the most modern approaches to deal with these model uncertainties and inaccuracies in the system is the robust control. Sliding mode control is an important robust control approach. It is a nonlinear control strategy. This control can tackle the parametric and modeling uncertainties of a nonlinear system. A sliding mode controller design provides a systematic approach to the problem of maintaining the stability and consistent performance in the face of modeling imprecision. In sliding mode control strategy, a smooth surface or manifold S is defined in the state space which represents a static relationship among the different state variables describing

the behavior of the system [17]. If these relationships are enforced on the dynamics describing the system, the reduced order dynamics may contain highly desirable features. The idea is to specify a feedback control action of variable structure switching nature, which guarantees reach ability of the prescribed manifold. Once the manifold conditions are met, it proceeds to maintain the systems motion constraints to this sliding surface ([18], [19] & [20]). A sliding mode control design has various design options. Stabilization problem (rest to rest maneuvers), nutation problem (a periodic behavior of state variables), tracking problem (to achieve the desired values of the state variables), de-tumbling and constant spinning are also within the scope of this method with minor modifications.

4.2.1 Dynamics and kinematics with MRPs

For a spacecraft attitude we use Modified Rodrigues parameters for the development of sliding mode controller. A non-linear model for the spacecraft motion is given [17] as

$$\dot{\bar{p}} = F(\bar{p}) \cdot \bar{\omega} \quad (\text{Kinematic Equations}) \quad (4.2)$$

$$\dot{\bar{\omega}} = f(\bar{\omega}) + I^{-1}\bar{T} + I^{-1}\bar{T}_d \quad (\text{Dynamic Equations}) \quad (4.3)$$

where $I \in \mathbb{R}^{3 \times 3}$ is the constant, positive definite and symmetric inertia matrix, $\bar{\omega} = [\omega_1, \omega_2, \omega_3]^T$ is the angular velocity vector, $\bar{T} = [T_1, T_2, T_3]^T$ is the control torque and $\bar{T}_d = [\bar{T}_{d1}, \bar{T}_{d2}, \bar{T}_{d3}]^T$ is the total external disturbance torque. The dynamic matrix and kinematic vector are defined as

$$F_{3 \times 3}(\bar{p}) = \frac{1}{4} \{ (1 - \bar{p}^T \bar{p}) I_{3 \times 3} + 2[\bar{p}^\times] + 2\bar{p}\bar{p}^T \} \quad (4.4)$$

$$f_{3 \times 1}(\bar{\omega}) = I^{-1} [I\bar{\omega}^\times] \cdot \bar{\omega} \quad (4.5)$$

The cross product matrix $[\zeta^\times], \forall \zeta = [\zeta_1, \zeta_2, \zeta_3]$ is defined as

$$[\zeta^x] = \begin{bmatrix} 0 & -\zeta_3 & \zeta_2 \\ \zeta_3 & 0 & -\zeta_1 \\ -\zeta_2 & \zeta_1 & 0 \end{bmatrix}$$

Let us define a vector $\bar{s} = \bar{\omega} - \bar{m}(\bar{p})$ which is a sliding surface and under ideal condition the state trajectory moves onto the sliding manifold ($\bar{s} = \bar{0}$). The quantity $\bar{m}(\bar{p})$ is obtained using a desired vector field from desired kinematic relations and is given by

$$\bar{m}(\bar{p}) = F^{-1}(\bar{p})d(\bar{p}) \quad (4.6)$$

The quantity $d(\bar{p})$ is defined as

$$d(\bar{p}) = \Lambda(\bar{p} - \bar{p}_d) \quad (4.7)$$

where \bar{p}_d is the desired reference trajectory of MRPs, and Λ is a diagonal matrix with negative elements. The values of entries of Λ are chosen at the bases of performance of the system. This allows for decoupled sliding motion and exponential convergence towards the final desired orientation. The inverse of dynamics matrix is derived as

$$F^{-1}(\bar{p}) = 4(1 + \bar{p}^T \bar{p})^{-2} \{ (1 - \bar{p}^T \bar{p}) I_{3 \times 3} - 2[\bar{p}^x] \}$$

As
$$\bar{s} = \bar{\omega} - \bar{m}(\bar{p})$$

Therefore, from equations [4.2] and [4.3]

$$\dot{\bar{p}} = F(\bar{p})(\bar{s} + \bar{m}(\bar{p}))$$

Also,

$$\dot{\bar{s}} = \dot{\bar{\omega}} - \frac{\partial \bar{m}}{\partial \bar{p}} \dot{\bar{p}}$$

$$\dot{\bar{s}} = f(\bar{\omega}) + I^{-1} \bar{T} - \frac{\partial \bar{m}}{\partial \bar{p}} F(\bar{p}) \bar{\omega}$$

$$\dot{\bar{s}} = f(\bar{\omega}) + I^{-1} \bar{T} - \frac{\partial \bar{m}}{\partial \bar{p}} [F(\bar{p})(\bar{s} + \bar{m}(\bar{p}))]$$

Clearly, for remaining on the surface ($\bar{s} = \bar{0}$), the control law is

$$\bar{T} = -I \left\{ f(\bar{\omega}) - \frac{\partial \bar{m}}{\partial \bar{p}} [F(\bar{p})(\bar{s} + \bar{m}(\bar{p}))] \right\} \quad (4.8)$$

To minimize chattering, the saturation function is added in the control law. This function is defined by

$$sat(s_i, \varepsilon) = \begin{cases} 1 & \text{for } s_i > \varepsilon \\ \frac{s_i}{\varepsilon} & \text{for } \|s_i\| \leq \varepsilon \\ -1 & \text{for } s_i < -\varepsilon \end{cases}$$

where ε is a small positive number. Finally, the control law becomes

$$\bar{T} = -I \left\{ f(\bar{\omega}) - \frac{\partial \bar{m}}{\partial \bar{p}} [F(\bar{p})(\bar{s} + \bar{m}(\bar{p}))] + K sat(s_i, \varepsilon) \right\} \quad (4.9)$$

Where $K_{3 \times 3}$ is a positive definite, diagonal matrix.

What is Chattering ?:

For an ideal sliding mode is that it exists only when the state trajectory of controlled spacecraft coincides with the desired trajectory at every time $t \geq t_1$ for some t_1 . This may require infinitely fast switching. The representative point is then oscillates within neighborhood of the switching surface. This phenomenon is called chattering.

Stabilization Problem:

In stabilization or regulation problem, the final position of a spacecraft is taken to be zero (i.e. unity quaternion). The corresponding MRPs are also taken to be zero as $\bar{p}_d = 0$. Also, the matrix Λ is taken as scalar λ times the identity matrix. Then,

$$\begin{aligned}\bar{m}(\bar{p}) &= F^{-1}(\bar{p})\lambda I_{3 \times 3} d(\bar{p}) \\ &= 4\lambda(1 + \bar{p}^T \bar{p})^{-2} \{(1 - \bar{p}^T \bar{p})I_{3 \times 3} - 2[\bar{p}^\times] + 2\bar{p}\bar{p}^T\} \bar{p}\end{aligned}$$

Differentiating w.r.t \bar{p}

$$\frac{\partial \bar{m}}{\partial \bar{p}} = 4\lambda(1 + \bar{p}^T \bar{p})^{-1} \{I_{3 \times 3} - 2(1 + \bar{p}^T \bar{p})^{-1} \bar{p}\bar{p}^T\} \quad (4.10)$$

Tracking Problem:

Requirement for the tracking problem is to follow a desired reference trajectory of MRPs (or Euler angles). The function $\bar{m}(\bar{p})$ has the following form for the tracking problem

$$\begin{aligned}\bar{m}(\bar{p}) &= 4\lambda(1 + \bar{p}^T \bar{p})^{-1} \bar{p} - 4\lambda(1 + \bar{p}^T \bar{p})^{-2} \dots \\ &\quad \{(1 - \bar{p}^T \bar{p})I_{3 \times 3} - 2[\bar{p}^\times] + 2\bar{p}\bar{p}^T\} \bar{p}_d\end{aligned}$$

The partial derivative of the above equation w.r.t \bar{p} yields

$$\begin{aligned}\frac{\partial \bar{m}}{\partial \bar{p}} &= 4\lambda(1 + \bar{p}^T \bar{p})^{-1} \{I_{3 \times 3} - 2(1 + \bar{p}^T \bar{p})^{-1} \bar{p}\bar{p}^T\} \\ &\quad - 8\lambda(1 + \bar{p}^T \bar{p})^{-2} \{\bar{p}\bar{p}_d^T - \bar{p}_d^T \bar{p} + [\bar{p}_d^\times] + (\bar{p}_d^T \bar{p})I_{3 \times 3}\} \\ &\quad + 16\lambda(1 + \bar{p}^T \bar{p})^{-3} \{(1 - \bar{p}^T \bar{p})I_{3 \times 3} - 2[\bar{p}^\times] + 2\bar{p}\bar{p}^T\} \bar{p}_d \bar{p}^T\end{aligned} \quad (4.11)$$

4.2.2 Lyapunov's Stability

Lyapunov analysis is used to check the stability of the sliding vector \bar{s} . Lyapunov method is usually used to determine the stability of an equilibrium point without solving the state equations. For Lyapunov stability we have to define an equilibrium point and state the Lyapunov's First or Direct Method.

Definition: The equilibrium point $x = 0$ of a nonlinear system $\dot{x} = f(x)$ is

(1) Stable if, for each $\varepsilon > 0$, there exist $\delta = \delta(\varepsilon)$ such that

$$\|x(0)\| < \delta \Rightarrow \|x(t)\| < \varepsilon, \forall \varepsilon \geq 0$$

(2) Unstable if not stable.

(3) Asymptotically stable if it is stable and δ can be chosen such that

$$\|x(0)\| < \delta \Rightarrow \lim_{t \rightarrow \infty} x(t) = 0$$

Lyapunov Analysis

The sliding vector $\bar{s} = \bar{\omega} - \bar{m}(\bar{p})$ can be shown using Lyapunov analysis. Consider the Lyapunov function candidate

$$V(\bar{s}) = \frac{1}{2} \bar{s}^T \bar{s}, \Rightarrow V(\bar{s}) \geq 0 \forall \bar{s}$$

$$(1) V(0) = 0 \text{ and } V(\bar{s}) > 0, \forall \bar{s} \in D \setminus \{0\}$$

$$(2) \dot{V}(\bar{s}) \leq 0, \forall \bar{s} \in D, \text{ then } \bar{s} = 0 \text{ is stable.}$$

and

$$(3) \text{ If } \dot{V}(\bar{s}) < 0, \forall \bar{s} \in D \setminus \{0\}, \text{ then } \bar{s} = 0 \text{ is asymptotically stable.}$$

In other word if a function $V(\bar{s})$ is positive definite and its derivative is negative definite for all x then this assures the stability of the system.

Proof:

Differentiating $V(\bar{s})$ w.r.t t

$$\begin{aligned}
\dot{V} &= \bar{s}^T \dot{\bar{s}} \\
&= \bar{s}^T \left[\dot{\bar{\omega}} - \frac{\partial \bar{m}}{\partial \bar{p}} \dot{\bar{p}} \right] \\
&= \bar{s}^T \left(f(\bar{\omega}) + I^{-1} \bar{T} - \frac{\partial \bar{m}}{\partial \bar{p}} F(\bar{p}) \bar{\omega} \right) \quad (4.12)
\end{aligned}$$

The control law is defined as:

$$\begin{aligned}
\bar{T} &= -I \left\{ f(\bar{\omega}) - \frac{\partial \bar{m}}{\partial \bar{p}} [F(\bar{p})(\bar{s} + \bar{m}(\bar{p}))] + K_{sat}(s_i, \varepsilon) \right\} \\
I^{-1} \bar{T} &= -f(\bar{\omega}) + \frac{\partial \bar{m}}{\partial \bar{p}} [F(\bar{p})(\bar{s} + \bar{m}(\bar{p}))] - K_{sat}(s_i, \varepsilon)
\end{aligned}$$

Substituting in Equ (4.12)

$$\dot{V} = -\bar{s}^T K_{sat}(s_i, \varepsilon)$$

This implies that

$$\dot{V} \leq 0, \quad \forall \bar{s}$$

◇

Chapter 5

5. Simulation Results

5.1 Simulation Results

The analysis of solar radiation pressure and forces shows that the solar radiation forces and rotational torques, produced by the cm/cp offset, using control boom mechanism and four control vanes mechanism produces the small rotational torques of order 1N-m and acceleration of order 10^{-6} deg/s². For different mission tasks like orbit raising, orbit maintenance and maneuvering of solar panel etc. we need large angular maneuvers. For this purpose, we have small rotational torques and large moments of inertia of the solar sail due to its larger size. Following three tables give solar sail characteristics. Table 3 shows sail characteristics, table 4 shows the attitude control characteristics while the simulation parameters are given in table 5.

Table 3-Solar Sail Characteristics

Solar Sail Size	40m × 40m
Payload Mass	$m_p=116$ Kgs
Sail Mass	$m_s= 40$ Kgs
Control Boom Length	$l= 30$ m
Distance of the vans from center of Sail	$d= 50$ m
Solar Pressure	$P= 4.563 \times 10^{-6}$ N/m ²
Solar Force	$F= 11.6 \times 10^{-3}$ N

Table 4- Attitude Control Characteristics

Inertia Matrix	$I = \begin{bmatrix} 6000 & 0 & 0 \\ 0 & 3000 & 0 \\ 0 & 0 & 3000 \end{bmatrix}$
Yaw Control Torque by Boom	0.2587 Nm
Pitch Control Torque by Boom	0.2587 Nm
Roll Control Torque by 4 Vans	0.8924 Nm
Pitch Control Torque by 4 Vans	1.1586 Nm

Table 5- Simulation Parameters

Initial Euler Angles	Yaw = 10 deg Pitch = 10 deg Roll = 10 deg
Initial Angular Velocities	$\omega_1 = 0$ rad/s $\omega_2 = 0$ rad/s $\omega_3 = 0$ rad/s
Desired Euler Angles before 150 Sec	Yaw = 0 deg Pitch = 0 deg Roll = 0 deg
Desired Euler Angles after 150 Sec	Yaw = 0 deg Pitch = 60 deg Roll = 0 deg
Constant Disturbance Torques	$T_{d1} = 0.15$ Nm $T_{d2} = -0.20$ Nm $T_{d3} = 0.30$ Nm

Two controllers, PD controller and sliding mode controller are used to simulate this tracking problem. PD controller results are taken for the saturation limit of rotational torque at 1Nm. The natural frequency and damping factor of the controller are chosen to be $\omega_n = 0.06$ and $\xi = 0.9$ giving the proportional and the derivative gain vectors as

$K_p = K = I\omega_n^2$ and $K_d = C = 2I\xi\omega_n$ respectively. The numerical values of the gain vectors are $K=[21.6 \ 10.8 \ 10.8]$ and $C=[648 \ 324 \ 324]$. Plots of closed loop trajectories of torques, angular velocities and Euler angles are given in Fig. 17, Fig. 18 and Fig. 19 respectively.

Constant external disturbance torques used in simulation are 15% of yaw torque, 20% of pitch torque and 30% of roll torque. Due to these disturbance torques, we can see a steady state error in all Euler angles. This agrees with the theory of PD controller.

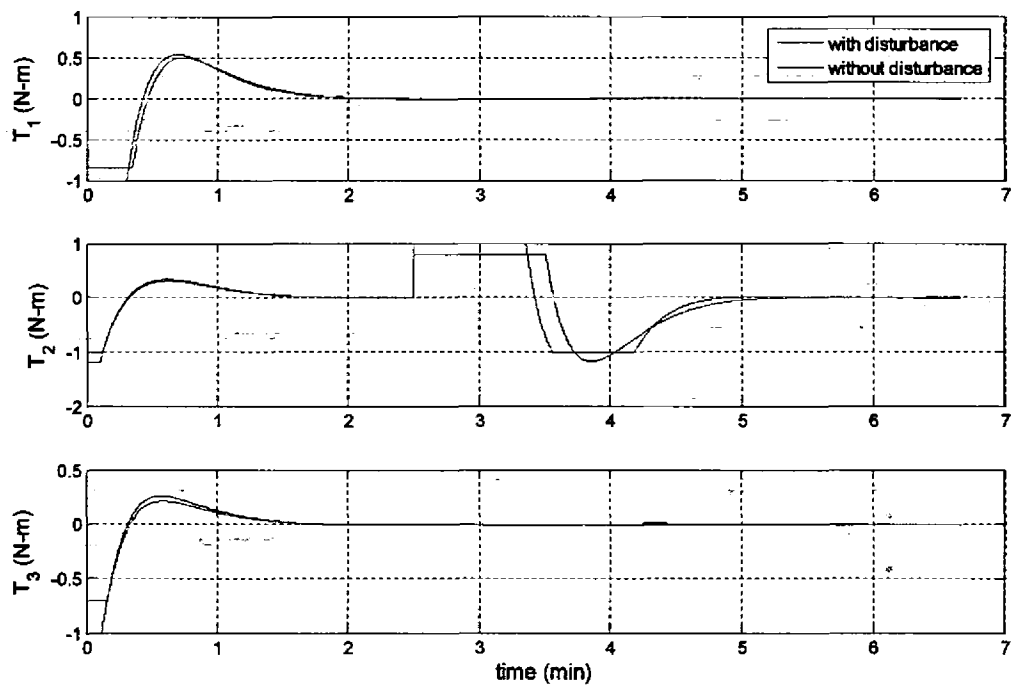


Figure 17-PD Controller torques

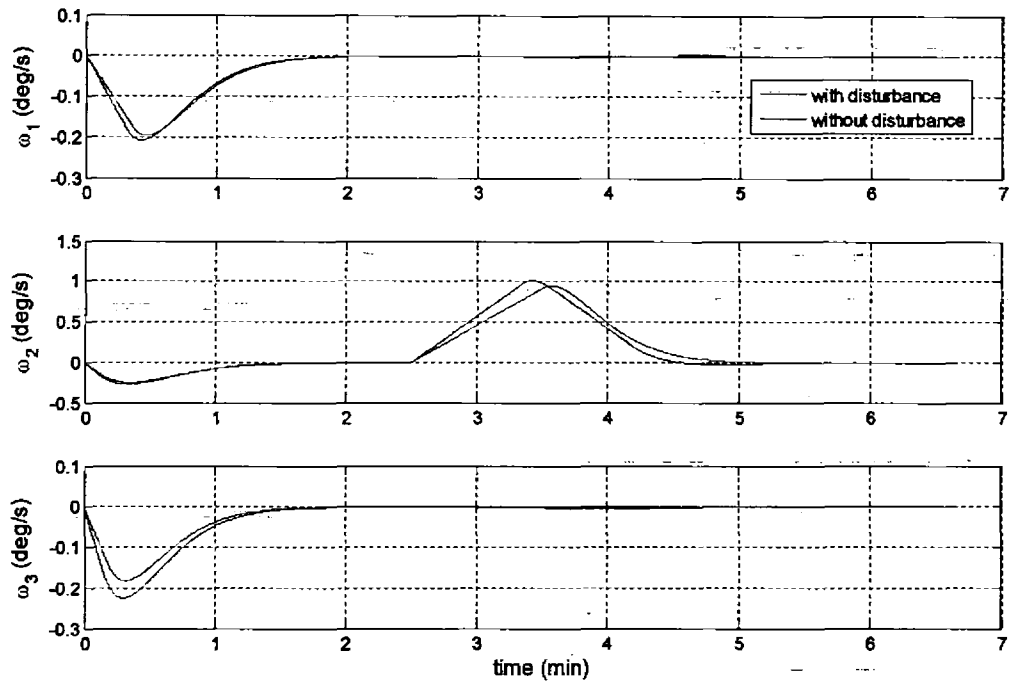


Figure 18- PD Controller Angular Velocities

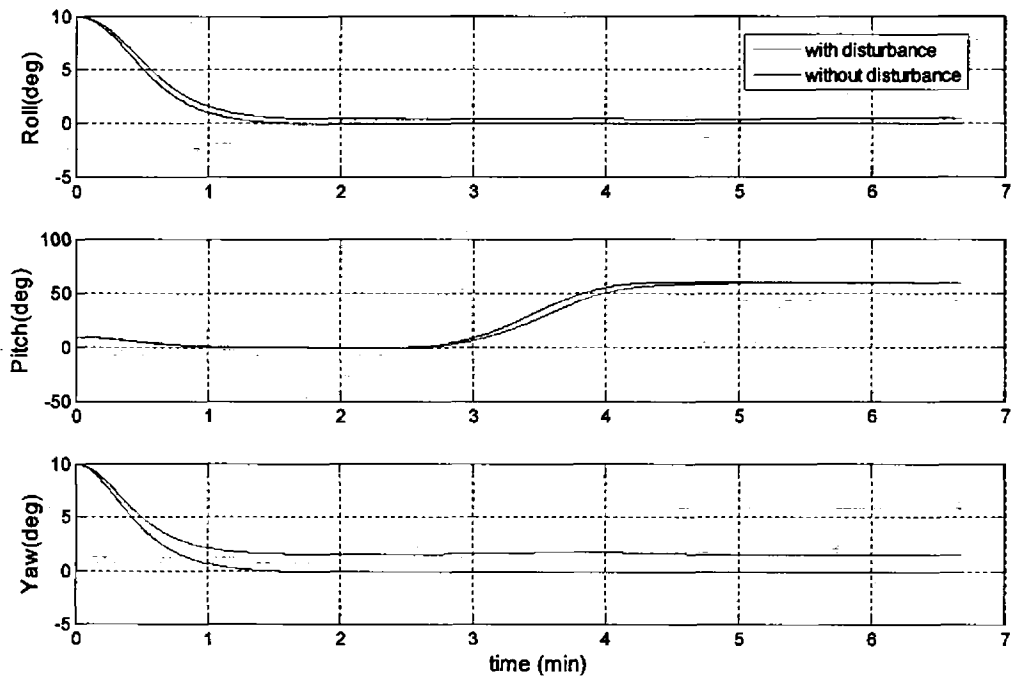


Figure 19- PD Controller Euler Angles

The sliding mode controller is tested and compared with PD controller for the same tracking problem as described above. A sliding mode controller is developed based on

the modified Rodrigues parameters. The initial conditions for the modified Rodrigues parameters are given by $[0.0397 \ 0.0473 \ 0.0397]$ which are converted from Euler angles $\psi = 10^\circ, \theta = 10^\circ$ and $\phi = 10^\circ$. The conversion of the Euler angles to the modified Rodrigues parameters is done via the function *eulerang2mrp.m*. Finally, the tracking results in the form of Euler angles are obtained from the MATLAB routine *mrp2eulerang.m*. The desired Euler angles are set to zero and the corresponding MRPs before 150 seconds are $p(t=0)=[0 \ 0 \ 0]$. After 150 seconds, the desired pitch angle is set to 60 deg while the yaw and roll angles are kept zero. The corresponding MRPs then come out to be $p(t \geq 150)=[0 \ 0.2679 \ 0]$. The diagonal elements of K in Equ. (4.9) are all set to value 1.0. The constant λ is set to - 0.07. The parameter ε , in the saturation function, in the control law is chosen as 0.01. It suitably covers the chattering problem in the control profile. The closed loop MRPs are shown in fig.19. The plots of MRPs, applied control torque trajectories, angular velocities, and tracking trajectories of Euler angles, with and without external torque disturbances, are shown in Fig. 20, Fig. 21 Fig 22 and Fig. 23 respectively. This shows the capability of the controller to overcome the model uncertainties and external disturbances.

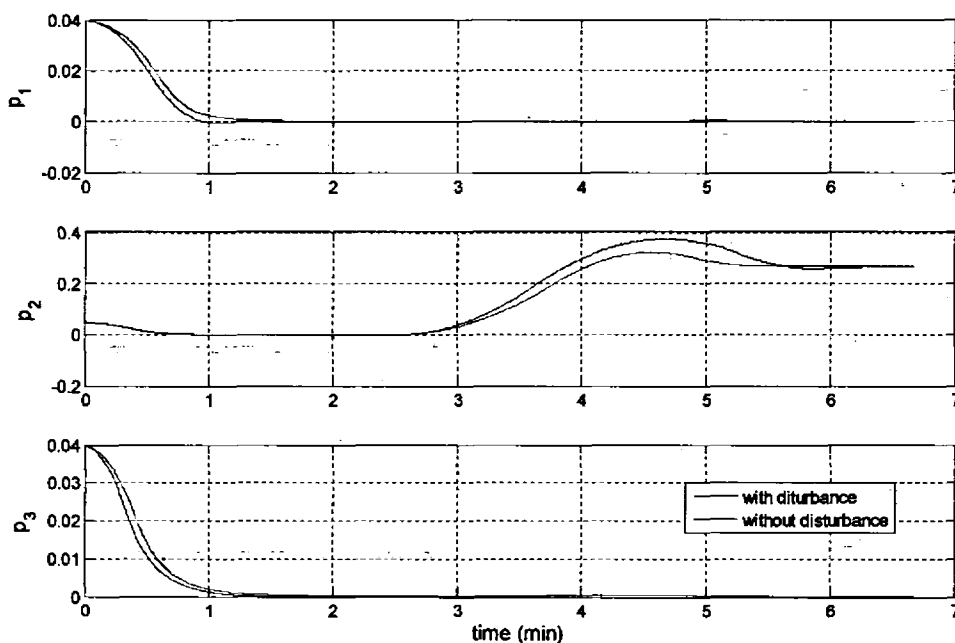


Figure 20- Modified Rodrigues parameters

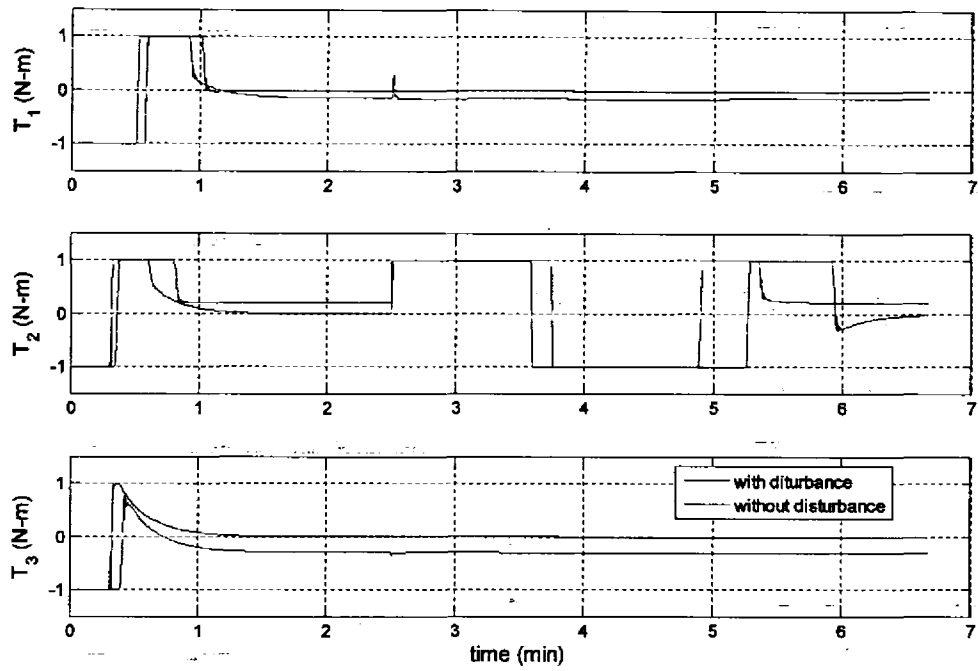


Figure 21 – Sliding Mode Torques

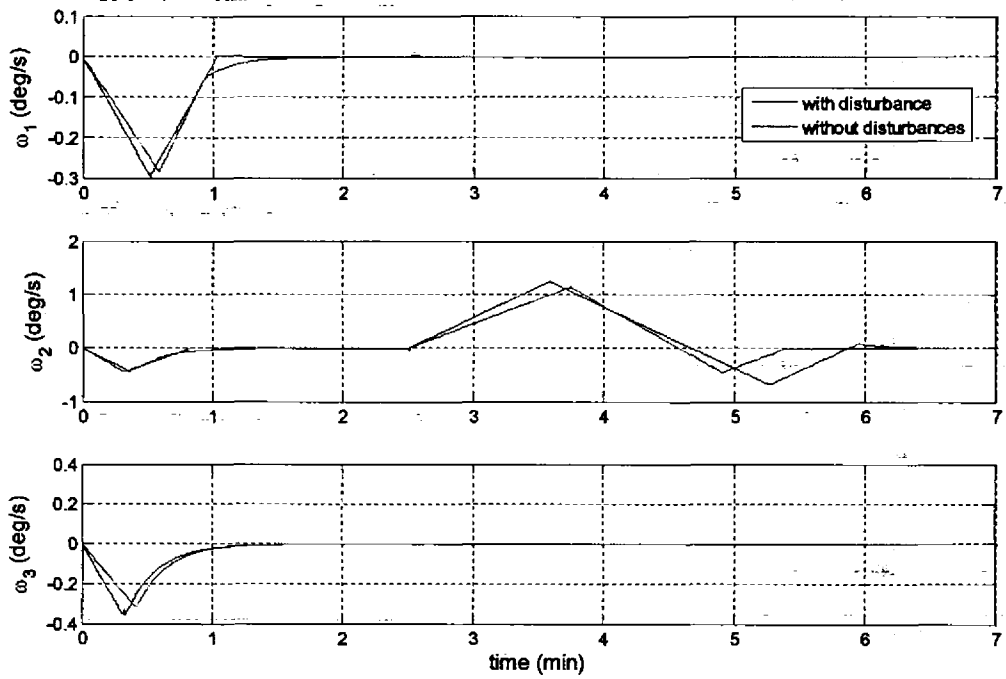


Figure 22- Sliding Mode Angular Velocities

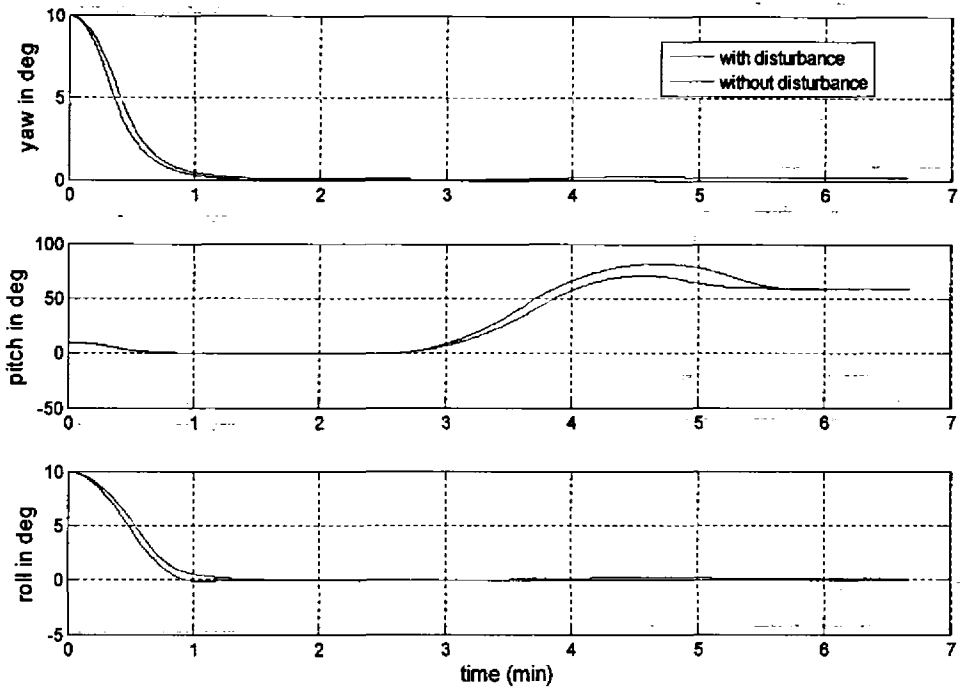


Figure 23 - Sliding Mode Euler Angles

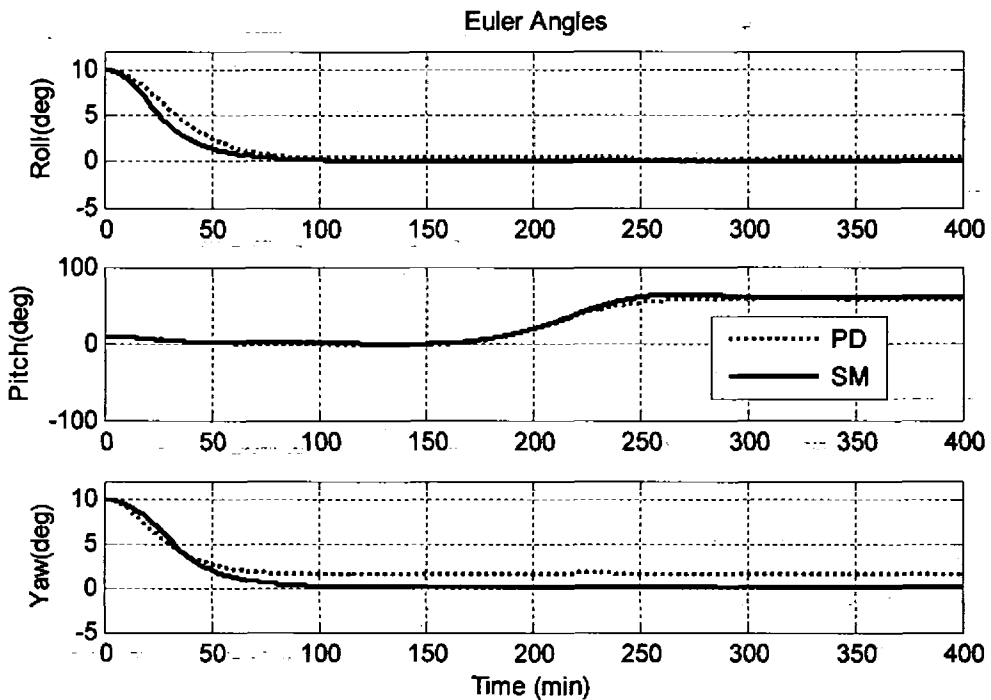


Figure 24 PD & SM Euler Angles with disturbances

In Fig. 24 euler angles tracking trajectories for both PD and sliding mode controller are compared. This proves the robustness of sliding mode as compare to PD control. Phase portraits of the state variables are shown in Figs. 25, 26 and 27 below:

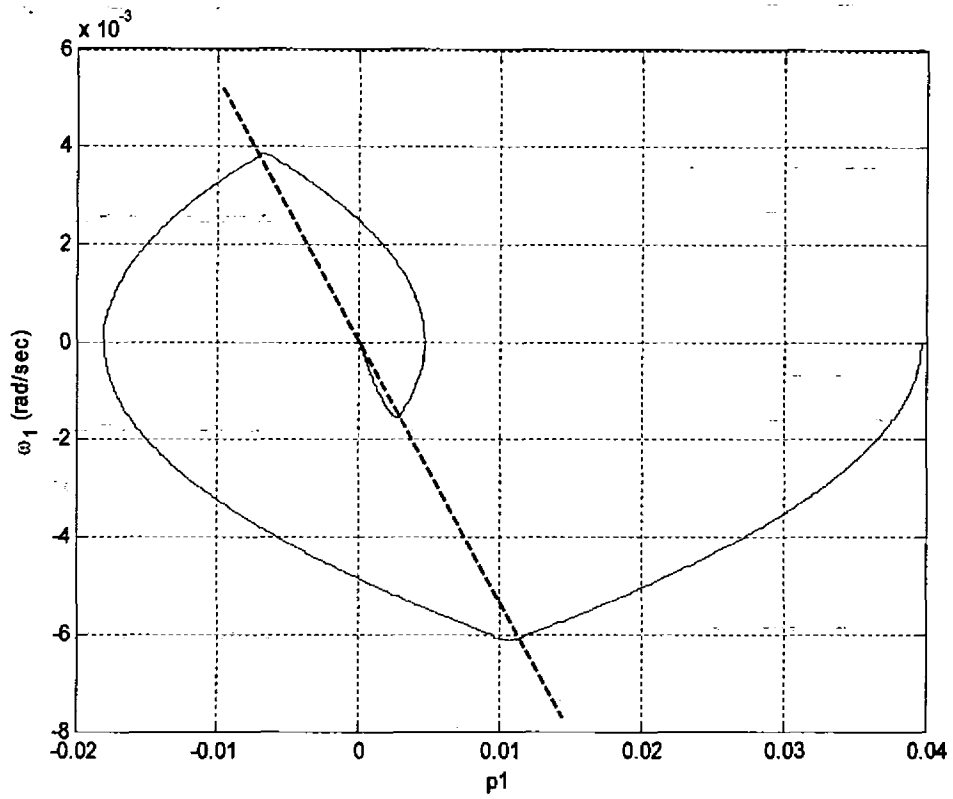


Figure 25- Phase Portrait ω_1 Vs p_1

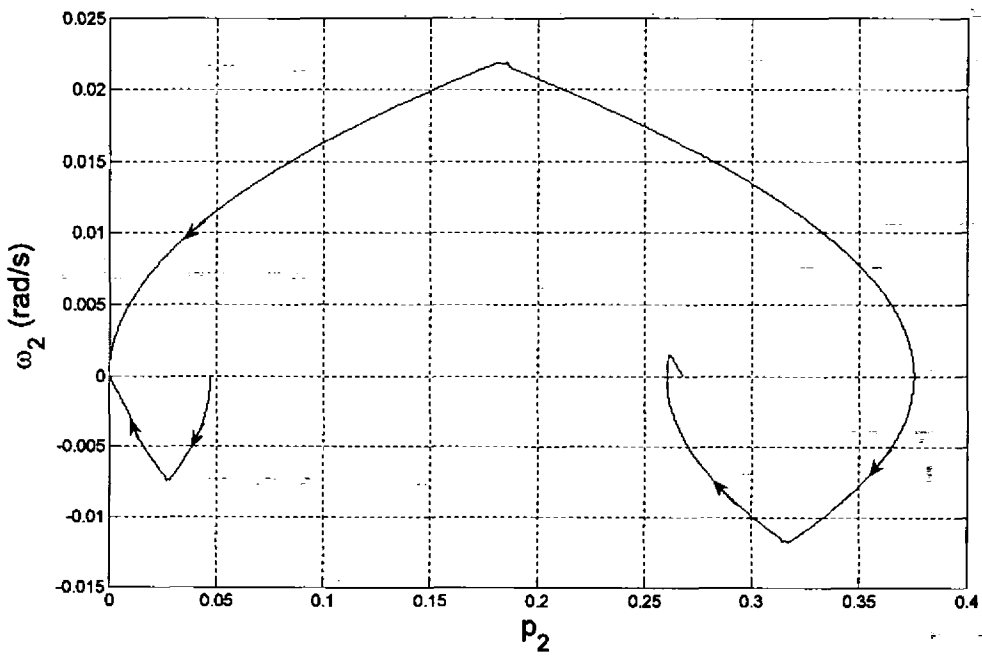


Figure 26 - Phase Portrait ω_2 Vs p_2

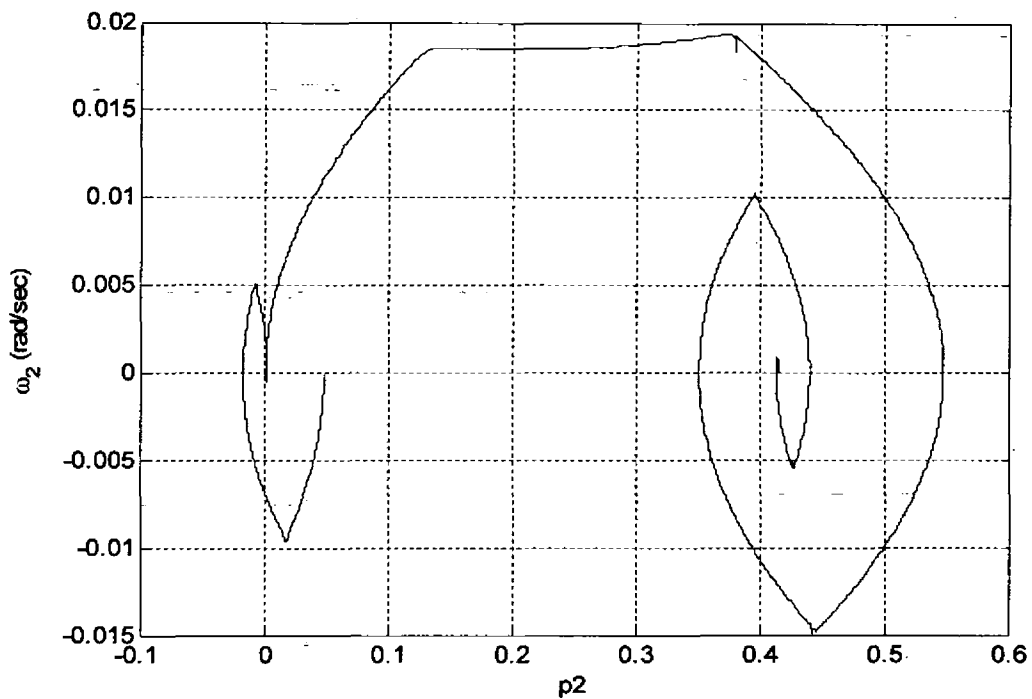


Figure 27 - Phase Portrait ω_2 Vs p_2 with $\epsilon = 0.005$

In Fig. 25 sliding line is shown. In Figure 27 chattering effect is shown for smaller value of ϵ . Sliding coordinates are shown in Figs. 28, 29 and 30. It is seen that they convert the tracking problem of state variable into a stabilization problem. Therefore, all sliding coordinates must settle to zero as shown in figures.

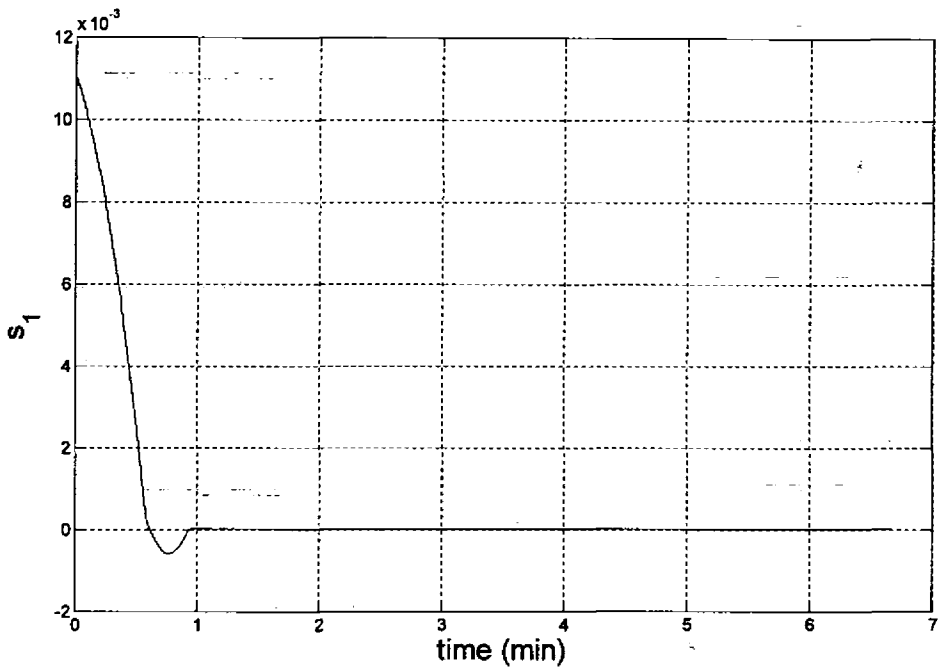


Figure 28 – Sliding Coordinate S_1 Vs time

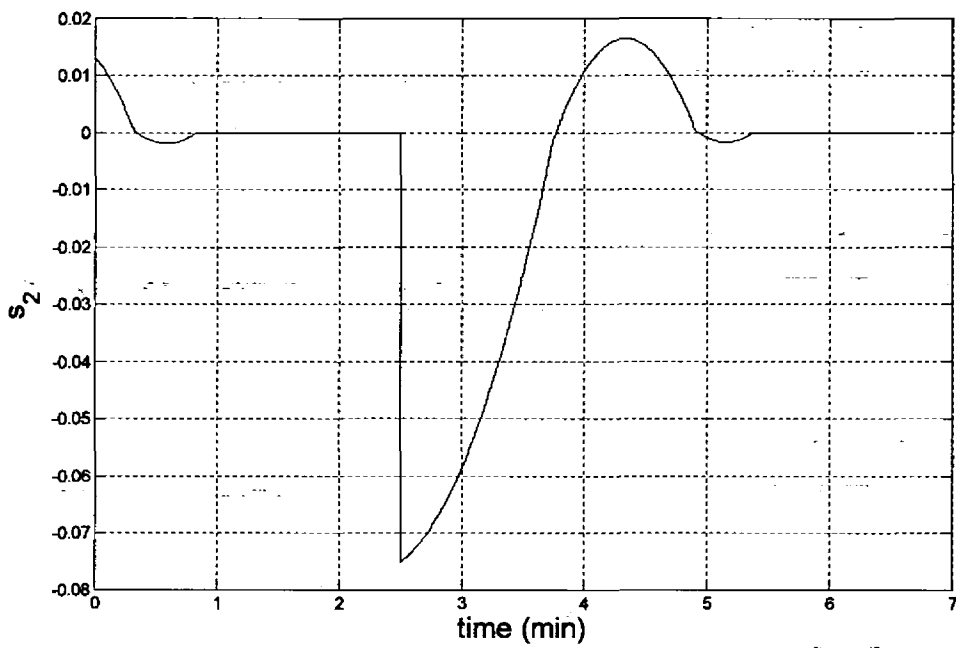


Figure 29– Sliding Coordinate S_2 Vs time

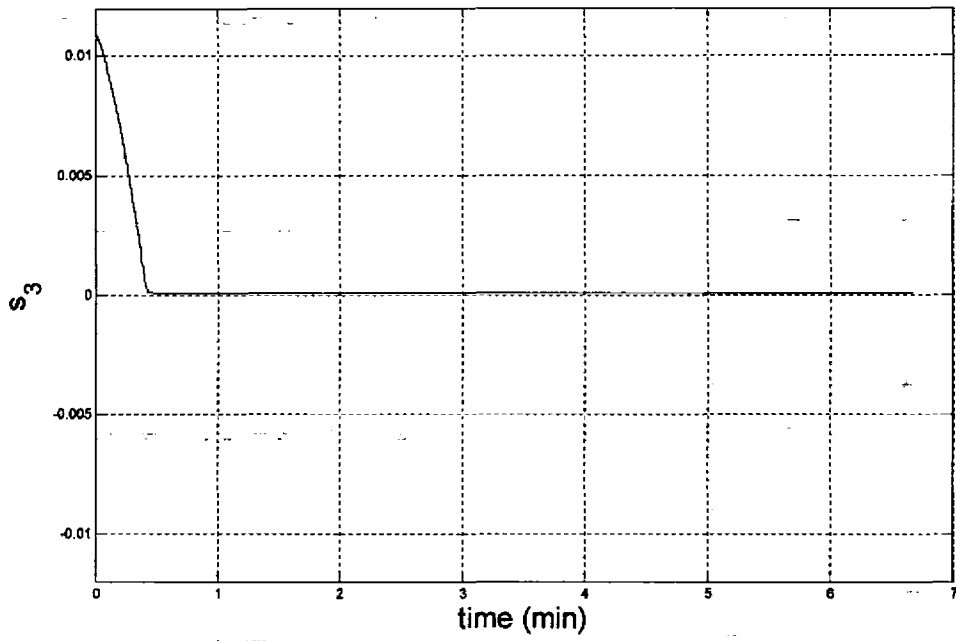


Figure 30– Sliding Coordinate S_3 Vs time

Chapter 6

6. Conclusion and Recommendations for Further Research

6.1 Conclusion

In this dissertation, a PD controller and sliding mode controller are developed to simulate the tracking problem of spacecraft attitude maneuvering. Small rotational torques are produced by boom and vanes mechanism using solar radiation pressure and forces. These torques are used for large angle maneuvering. The provided torques are in the limits of 1.0 N-m.

PD controller is used for the torque of 1.0 N-m. It has given smoother trajectories of torque and angular velocities. There is no chattering issue has been seen in the torque and angular velocity profiles. Lesser switching took place in the control torques generated by the PD controller as compare to sliding mode controller. For PD controller we used Euler angles. The disadvantages of the PD controller are singularities for the large angle maneuvers. For example, the singularities occur at 90° and 270° in the pitch angle maneuvering. So we cannot use it for pitch maneuvering greater 90° . It has been validated through the simulation. Proportional gain and derivative gain adjustment is also difficult. On the other hand, the sliding mode controller uses the Modified Rodrigues parameters. The Modified Rodrigues parameter represent minimal parameterization as compare to quaternion representation with singularity only at 360° as compare to the Euler angle representation. Therefore, it is able to control the attitude of a spacecraft for large angular maneuvers.

There are two major advantages of the sliding mode controller over the PD controller. One is the auto gain adjustment and other is the transformation of higher order systems into first order sliding surface. The proportional and derivative gain

adjustment is a difficult problem in PD controller for non linear systems. Maneuvering rates, whether faster or slower, are decided as per these gains. Sliding mode controller is robust in comparison to the PD controller and has no such issue. We transform the original higher order tracking problem into a simple 1st order stabilization problem in the sliding surface parameter S . In the first order system, the intuitive control strategy is, 'if the error is negative, push is exerted in the positive direction and if the error is positive, push is exerted in the negative direction'. This characteristic of sliding mode control covers the uncertainties due to modeling and external disturbances from the environment. The disadvantage of sliding mode controller is high switching of the controller which causes chattering. This is not desirable, since it involves high control activity. It can be reduced by using different techniques. Robustness and computational simplicity of the controller recommends it for online applications.

6.2 Recommendations for future research

Different control techniques for spacecraft attitude control using solar radiation forces and torques have been studied in this dissertation, but some issues have not been addressed in details or at all. So it is suggested that these issues should be addressed in future research.

1. Actuator dynamics has not been used in the present studies and in the simulation results. Only a low torques of with the saturation limits of 1.0 N-m have been used. The actuators dynamics and actual torques produces by this mechanism can also be used for attitude control
2. Due simplicity and robustness of sliding mode control technique, we can use it for on line problems as well.
3. These control technique are also suitable for internally produced torques like torques produced by thrusts, electric propulsion and momentum transfer reaction wheels.
4. Some mission specific application like earth pointing spacecraft in elliptic orbits, sun pointing spacecraft in elliptic orbits, orbit maintenance and escape orbit trajectories can also be solved using these techniques.

References

- [1]. Stephanie D. Leifer, "The NASA Advanced Propulsion Concepts Program", 33rd Joint Propulsion Conference, 1997.
- [2]. Bong Wie, "Space Vehicle Dynamics and Control", Second Edition AIAA Education Series, 2008.
- [3]. G. Greschik and M. M. Mikulas, "Design Study Of a Square Solar Sail Architecture", *Journal Of Spacecraft And Rockets* Vol. 39, No. 5, 2002.
- [4]. Bong Wie, "Dynamic Modeling and Attitude Control of Solar Sail Spacecraft", AIAA Guidance, Navigation and Control Conference August 2002, Monterey.
- [5]. Mc. Innes, C. R., "Solar Sailing, Technology, Dynamics and Mission Applications", Springer Praxis Publishing, 1999.
- [6]. West, J. L. And Derbes, B., "Solar Sail Vehicle System Design for The Geostorm warning Mission," AIAA 2000-5326, Presented at The AIAA Space 2000 Conference, Long Beach, Ca, Sept. 20-21, 2000.
- [7]. Renner, U. "Attitude Control by Solar Sailing: A Promising Experiment with Ots-2", *European Space Agency Journal*, Vol. 3, No. 1, 1979, pp. 35-40.
- [8]. Lievre, J., "Solar Sailing Attitude Control of Large Geostationary Satellite", *Ifac Automatic Control In Space*, Pergammon, Oxford, Uk, 1985, pp. 29-33.
- [9]. Guido Colasurdo, "Optimal Control Law for Interplanetary Trajectories with Non-ideal Solar Sail", *Journal Of Spacecraft And Rockets*, Vol. 40, No. 2, March-April 2003.
- [10]. J.C. Van Der Ha , V.J. Modit, "Orbital Perturbations And Control By Solar Radiation Forces", *J. Spacecraft* , Vol. 15, No. 2, March-April 1978.
- [11]. S.K. Shrivastava, "Optimum Orbital Control Using Solar Radiation Pressure", *Engineering Notes* August 1975.
- [12]. Berned Dachwald, "Interplanetary Mission Analysis for Non-Perfect Reflecting Solar Sail craft using Evolutionary Neurocontrol", *Astrodynamics Specialist Conference 2004*, Montana , San Diego, CA 92198 :Paper AAS 03-579.
- [13]. A. F. D'Souza and V. K. Garg, "Advanced Dynamics Modeling and Analysis", Prentice-Hall INC., Englewood Cliffs, New Jersey 1984.

- [14]. J. H. Ginsberg and J. Genin, "Dynamics", 2nd Edition, John Wiley & Sons, New York, 1984.
- [15]. T. S. Jayarman, "Time-Optimal Orbit Transfer Trajectory for Solar Sail Spacecraft", J. Guidance and Control Vol. 3, No: 6 Article No. 80-4121.
- [16]. Bong Wie, "Thrust Vector Control of Solar Sail Spacecraft", AIAA Guidance, Navigation and Control Conference, August 2005, Monterey.
- [17]. Bong Wie, "Solar-Sail ACS Development for a Sail Flight Validation Mission in a Sun-Synchronous Orbit", AIAA Journal Of Spacecrafts And Rockets, February 2006.
- [18]. Crassidis, J.L., Markley, F.L., "Sliding Mode Control Using Modified Rodrigues Parameters", Journal of Guidance, Control and Dynamics, Vol. 19, NO. 6 Nov-Dec. 1996. pp.262-270.
- [19]. Ramirez, H.S., Dwyer, T.A.W., "Variable Structure Control of Spacecraft Reorientation Maneuvers", Journal of Guidance, Control and Dynamics, Vol. 11, NO. 3 May-June 1988. pp. 262-270.
- [20]. Vadali, S.R., "Variable Structure Control of Spacecraft Large Angle Maneuvers", Journal of Guidance, Control and Dynamics, Vol. 9, No.2, March-April 1986, pp. 235-239.
- [21]. Utkin, V.I., "Variable Structure System with Sliding Mode", IEEE – "Transactions on Automatic Control", Vol. AC-22, No. 2, April 1977, pp. 212-222.
- [22]. Lo, S.C., Chen, Y.P., "Smooth Sliding Mode Control for Spacecraft Attitude Maneuvers", Journal of Guidance, Control and Dynamics, Vol. 19, NO. 6 Nov-Dec. 1996. pp.262-270.
- [23]. Jovan, D.B., Li, S.M., "Robust Adaptive Variable Structure Control of Spacecraft under Control Input Saturation", Journal of Guidance, Control and Dynamics, 2001, 24(1): 14-22.
- [24]. M. J. Sidi, "Spacecraft Dynamics and Control: A Practical Engineering Approach", Cambridge University Press, New York, 1997.
- [25]. S. Varma, K.D. Kumar "Fault Tolerant Satellite Attitude Control using Solar Radiations Pressure Based on non-linear adaptive sliding mode" (Acta Astronautica Vol. 66 issues 3-4 Feb.- March,2010 pages: 486-500)

- [26]. T.R Patel, K.D Kumar, K. Behdinan," Satellite Attitude Control using Solar Radiation Pressure Based on non-linear Sliding Mode Control" *Journal of aerospace Engineering* March 1-2008, 222:379-392, doi:1234/09544100JAER0269

APPENDIX

MATLAB Code for Simulations Performed for Solar Torques and Forces Generation

M- File

```
% This program generates three axis stabilized torque on
%solar sail using boom
r2d = 180/pi;
mp = 116; % Payload mass in kg
ms = 40; % solar sail mass in kg
len= 15; % Control boom length in meters
theta =0:0.1:pi/2;
phi    = 0:0.1:2*pi;
alpha = 0.0;
F = 11.6*10^-3;
for i =1:length(theta)
    for j=1:length(phi)
        Mx(i,j) = -
F*(mp/(mp+ms))*len*cos(alpha)^2*cos(theta(i))*sin(phi(j))
;
        My(i,j) = -
F*(mp/(mp+ms))*len*cos(alpha)^2*cos(theta(i))*cos(phi(j))
;
    end
end
tx_max = max(max(Mx))
tx_min = min(min(Mx))
ty_max = max(max(My))
ty_min = min(min(My))
figure(1)
```

```

surf(Mx);grid
xlabel('Boom Azimuth \phi (rad)');
ylabel('Boom elevation \theta (rad)');
zlabel('Pitch Torque \tau_x (N-m)');
figure(2)
surf(My);grid
xlabel('Boom Azimuth \phi (rad)');
ylabel('Boom elevation \theta (rad)');
zlabel('Yaw Torque \tau_x (N-m)');

```

M-File

```

clear all
clc
% This program generates three axis stabilized torque on solar sail
% using Control Vanes
r2d = 180/pi;
del1 = -pi/2:0.1:pi/2;
del2 = -pi/2:0.1:pi/2;
alpha = 0.0;
d = 28.28; % Distance from center of sail to vanes
F = 11.6*10^-3;
for i =1:length(del1)
    for j=1:length(del2)
My(i,j) = F*d*cos(alpha)^2*(cos(del1(i))^3 - cos(del2(j))^3);
Mz(i,j) = F*d*cos(alpha)^2*(cos(del1(i))^2*sin(del1(i))+
cos(del2(j))^2*sin(del2(j)));
    end
end
tz_max = max(max(Mz))
tz_min = min(min(Mz))
ty_max = max(max(My))
ty_min = min(min(My))
figure(1)
surf(My);grid

```

```

xlabel('Vane1 Rotation \delta_1 (rad)');
ylabel('Vane2 Rotation \delta_2 (rad)');
zlabel('Pitch Torque \tau_x (N-m)');
figure(2)
surf(My);grid
xlabel('Vane1 Rotation \delta_1 (rad)');
ylabel('Vane2 Rotation \delta_2 (rad)');
zlabel('Yaw Torque \tau_x (N-m)');

```

M- File

```

clear all
clc
%This Program gives Solar Radiation Force (SRF) vs sun
%angle(pitch angle)for a non-perfect sail of 40m by 40m
r2d = 180/pi;
Bf = 0.79; Bb = 0.55; % non-lambertian coefficients
ef = 0.05; eb = 0.55; % surface emission coefficients
r = 0.88; % reflectivity of front surface
s = 0.94; % specular reflection coefficient
P = 4.563*10^-6; % Solar Pressure in N/m^2
A = 40*40; % Sail Area
a = 0:0.01:pi/2;
Fn = P*A*((1+r*s)*cos(a).^2+Bf*r*(1-s)*cos(a)+(ef*Bf-
eb*Bb)*(1-r)*cos(a)/(ef+eb));
Ft = P*A*(1-r*s)*cos(a).*sin(a);
F = sqrt(Fn.^2 + Ft.^2);
max(F)
beta = atan2(Ft,Fn); % Angle of the force with surface
figure(1)
plot(a*r2d,Fn,'r',a*r2d,Ft,'r--',a*r2d,F);grid;shg

```

```

title ('Sun Angle Vs Normal,Tangential Force & Total
Forces')
xlabel('\alpha (deg)');ylabel('Forces (N-m)');
legend('Fn','Ft','F')
figure(2)
plot(beta*r2d);grid
title ('Angle b/w Net Force & Surface Normal')
xlabel('time (sec)');ylabel('\beta (deg)');

```

M-File

```

clear all
clc
% Payload vs square sail side when characteristic acc. is
% known. Taking Payload as 1/3 of the total mass of the sail

P0 = 4.563*10^-6; % solar radiation pressure at 1AU
eta = 0.85; % sail efficiency
mt =0:150;
ms = mt/3;
ca =[0.5 1 3 6]*1000; % characteristic acc. in m/s^2
figure
hold all
for i=1:length(ca)
    for j=1:length(mt)
        area = ca(i)*mt(j)/(2*eta*P0);
        side(j)=sqrt(area);
    end
    plot(ms,side/1000)
end
legend('0.5 mm.s^-2','1 mm.s^-2','3 mm.s^-2','6 mm.s^-2')
xlabel('Payload (kg)');
ylabel('Sail Side (m)');
hold off

```

MATLAB Code for Spin-Stabilization Simulation

Function File

```
% Function File of dynamic equations of solar sails spin
% stabilization
function out = Dynam_equ(t,x)
global J F epsi
d2r = pi/180;
w1 = x(1,1);
w2 = x(2,1);
w3 = x(3,1);
r = x(4,1);
p = x(5,1);
y = x(6,1);
T1=0;
T2=0;
T3=epsi*F;
w1dot = ((J(2) -J(3))*w2*w3 + T1)/J(1);
w2dot = ((J(3) -J(1))*w3*w1 + T2)/J(2);
w3dot = ((J(1) -J(2))*w1*w2 + T3)/J(3);
rdot = w1 + (w2*sin(r) + w3*cos(r))*tan(p);
pdot = w2*cos(r) - w3*sin(r);
ydot = (w2*sin(r) + w3*cos(r))/cos(p);
out = [w1dot;w2dot;w3dot;rdot;pdot;ydot];
```

M-File

```
clear all
clc
% Attitude control by spin stabilization using cm/cp offset
global J epsi F
d2r = pi/180;
r2d = 180/pi;
J = [6000;3000;3000]; % Inertia Matrix
```

```

Omega = 0.5;           % Spin axis angular Velocity in deg/s
epsi  = 0.1;          % cm/cp offset in meters
F     = 0.01;         % SRPF in Newtons
t_span = [0 2000];
%initial conditions for angular velocities and Euler angles
x0 = [Omega; 0; 0; 0; 0; 0]*d2r;
options=odeset('MaxStep',1);
[t,x] = ode45(@Dynam_SS,t_span,x0,options);
figure(1)
subplot(2,2,1)
plot(t,x(:,5)*r2d);grid
xlabel('time (sec)');ylabel('Pitch(deg)');
subplot(2,2,2)
plot(t,x(:,6)*r2d);grid
xlabel('time (sec)');ylabel('Yaw(deg)');
subplot(2,2,3)
plot(x(:,5)*r2d,x(:,6)*r2d);grid
xlabel('Pitch(deg)');ylabel('Yaw(deg)');
subplot(2,2,4)
plot(x(:,2),x(:,3)*r2d);grid
xlabel('\omega_2 deg/s');ylabel('\omega_3 deg/s');

```

MATLAB Code for Simulation with Sliding Mode Control

Function File

```

% Function Files used to convert Modified Rodrigues Parameters to
%Euler Angles and vice versa
function p = angle2mrp(ang)
d2r=pi/180;
ang = ang*d2r;
q = angle2quat(ang(1),ang(2),ang(3));
p = [q(1);q(2);q(3)]/(1+q(4));

%-----

```

```

function ang = mrp2angle(p)
r2d = 180/pi;
q4 = (1-(norm(p))^2)/(1+(norm(p))^2);
q1 = p(1)+p(1)*q4;
q2 = p(2)+p(2)*q4;
q3 = p(3)+p(3)*q4;
[yaw, pitch, roll] = quat2angle([q1,q2,q3,q4]);
ang = [yaw;pitch;roll]*r2d;

```

Function File

```

% Dynamics of sliding mode
function out = slidingmode_dyn(t,x)
global fid J K lemda epsi p_d
d2r = pi/180;
if( t > 150)
    p_d = [0.866025403784439;0;0.5];
end
w = [x(1,1); x(2,1); x(3,1)];
p = [x(4,1); x(5,1); x(6,1)];
Jw = J*w;
Jwx = [0 -Jw(3) Jw(2);Jw(3) 0 -Jw(1);-Jw(2) Jw(1) 0];
px = [0 -p(3) p(2);p(3) 0 -p(1);-p(2) p(1) 0];
pdx = [0 -p_d(3) p_d(2);p_d(3) 0 -p_d(1);-p_d(2) p_d(1) 0];
F = ((1-p'*p)*eye(3) + 2*px + 2*p*p')/4;
f = inv(J)*Jwx*w;
%-----Control Law ( for tracking)-----
term1 =lemda/(1+p'*p);
term2 =lemda/(1+p'*p)^2;term3=lemda/(1+p'*p)^3;
m = 4*term1*p - 4*term2*((1-p'*p)*eye(3) - 2*px + 2*p*p')*p_d;
delm1 = 4*term1*(eye(3)-2*p*p'/(1+p'*p));
delm2 = 8*term2*(p*p_d' -p_d*p'+pdx+(p_d'*p)*eye(3));
delm3 = 16*term3*((1-p'*p)*eye(3)- 2*px + 2*p*p')*p_d*p';
delm = delm1 - delm2 + delm3;
s = w - m;
for j=1:3
    if( s(j,1) > 0)

```



```

[t,x] = ode45(@slidingmode_dyn,t_span,x0,options);
fclose(fid);
load xd.dat
figure(1)
subplot(3,1,1)
plot(t,x(:,4));grid
xlabel('time (sec)');ylabel('p1');
subplot(3,1,2)
plot(t,x(:,5));grid
xlabel('time (sec)');ylabel('p2');
subplot(3,1,3)
plot(t,x(:,6));grid
xlabel('time (sec)');ylabel('p3');
figure(2)
subplot(3,1,1)
plot(t,x(:,1));grid
xlabel('time (sec)');ylabel('\omega_x (rad/s)');
subplot(3,1,2)
plot(t,x(:,2));grid
xlabel('time (sec)');ylabel('\omega_y (rad/s)');
subplot(3,1,3)
plot(t,x(:,3));grid
xlabel('time (sec)');ylabel('\omega_z (rad/s)');
figure(3)
subplot(3,1,1)
plot(xd(:,1),xd(:,2));grid
xlabel('time (sec)');ylabel('\tau_x (N-m)');
subplot(3,1,2)
plot(xd(:,1),xd(:,3));grid
xlabel('time (sec)');ylabel('\tau_y (N-m)');
subplot(3,1,3)
plot(xd(:,1),xd(:,4));grid
xlabel('time (sec)');ylabel('\tau_z (N-m)');
figure(4)
subplot(3,1,1)
plot(xd(:,1),xd(:,5));grid
xlabel('time (sec)');ylabel('yaw in deg');
subplot(3,1,2)

```

```
plot(xd(:,1),xd(:,6));grid
xlabel('time (sec)');ylabel('pitch in deg');
subplot(3,1,3)
plot(xd(:,1),xd(:,7));grid
xlabel('time (sec)');ylabel('roll in deg');
```